Aeolian Research 75 (2026) 101027

Contents lists available at ScienceDirect

Aeolian Research

journal homepage: www.elsevier.com/locate/aeolia

Full Length Article

The Sand AbrasioN Device for Aeolian Research (SANDAR): A new experimental device for investigating how wind transport affects sand on Earth and Mars

Anna E. Baker [a,*], Devon M. Burr [b], Rachel L. Fry [c,d], Joshua P. Emery [a], Mark J. Loeffler [a]

[a] Department of Astronomy and Planetary Science, Northern Arizona University. 527 S. Beaver St., Flagstaff, AZ 86011-6010, United States
[b] Formerly of Department of Astronomy and Planetary Science, Northern Arizona University. 527 S. Beaver St., Flagstaff, AZ 86011-6010, United States
[c] U.S. Geological Survey, Astrogeology Science Center. 2255 N. Gemini Drive, Flagstaff, AZ 86001, United States
[d] Department of Applied Physics and Materials Science, Northern Arizona University. 527 S. Beaver St., Flagstaff, AZ 86011-6010, United States

A B S T R A C T

On Earth and Mars, aeolian transport causes sand grains to become abraded, resulting in mineralogic and textural changes. Understanding how sands evolve, or mature, with transport via experimental studies is important for understanding the origins, geologic history, and cycling of sediments, as well as dust production. Previous experimental works have used a variety of methods to simulate aeolian transport in the laboratory, but practical limitations and similitude concerns have limited such research. Here, we present and validate the Sand AbrasioN Device for Aeolian Research (SANDAR), a modified air mill that uses pressurized air to circulate sand around a small abrasion chamber, simulating the effects of aeolian transport. This device is re-circulating to simulate long-distance transport, and it allows for repeated analyses of well-constrained sediment samples, revealing their evolution over time. It is compatible with the grain sizes (74–500 μm) and grain impact velocities (~0.6–3.7 m/s) typically expected for natural aeolian environments, and is also adaptable for diverse applications simulating different wind conditions. We show that the SANDAR achieves similitude of kinetic energy with respect to saltating sand on both Earth and Mars. SEM and optical microscope imaging reveal that the SANDAR produces microtextures on the surfaces of sand grains similar to those found with natural aeolian transport, demonstrating that it effectively simulates the mechanical effects of aeolian processes. Thus, the SANDAR is a valid tool for use in experimental research to improve our understanding of sedimentary processes across the Solar System.

1. Introduction

Understanding how aeolian transport affects sediments is key to understanding sedimentary cycles and surface processes on Earth, Mars, and other planetary bodies. When sand is transported by wind, it moves primarily via saltation, in which sand grains make long hops and repeatedly collide with other loose sand grains at the bed surface. A secondary mechanism is creep, in which sand grains move while staying in contact with the bed surface (Bagnold 1941). During these processes, interactions between sand grains result in mechanical abrasion of the grains, which can cause morphological and mineralogical changes known as sediment maturation. Morphological changes include chipping or fracturing, rounding, attrition and comminution (particle size reduction), and the development of microtextures on the surfaces of grains (e.g., Anderson, 1926; Kuenen, 1960a; Krinsley and Takahashi, 1962). Mineralogical changes occur due to the differential abrasion rates of different minerals in a sediment; on Earth, felsic sands that undergo aeolian transport tend to be enriched in quartz and depleted in feldspars, carbonates, and clay minerals (e.g., Pettijohn et al., 1972; Blatt, 1973).

The aeolian abrasion of sediments has significant implications for several processes in sedimentology, making it an important subject for research. First, aeolian abrasion rates determine how much transport a sediment can withstand before it is mechanically broken down into sub-sand grain sizes (<62.5 μm). This concept of sand survivability places limits on the scale and duration of source-to-sink sediment transport cycles (e.g., Rogers and Christensen, 2003). Second, if sediment maturation is well understood, sand mineralogy and texture can be used to help inform research on the provenance and geologic history of sediments in dune fields or sandstones (Nesbitt and Young, 1996; Muhs, 2004; Olivarius et al., 2022; Marvin et al., 2025). Third, the chipping and comminution of saltating sand grains results in the production of dust- and silt-sized materials (e.g., Whalley et al., 1987; Bullard et al., 2004; Crouvi et al., 2008; Sweeney et al., 2023). Understanding this process is important for understanding and predicting dust hazards, particularly in the context of Earth's changing climate (e.g., Crouvi et al., 2012; Middleton, 2017).

* Corresponding author..
E-mail address: Aeb566@nau.edu (A.E. Baker).

https://doi.org/10.1016/j.aeolia.2025.101027
Received 10 August 2025; Received in revised form 2 December 2025; Accepted 16 December 2025
Available online 5 January 2026

Our knowledge of the effects of aeolian abrasion is highly dependent on laboratory experimental studies (e.g., Anderson, 1926; Kuenen, 1960a; Rasmussen et al., 2015) because the physics of sand is difficult to conceptualize theoretically due to the complex nature of granular materials (e.g., Dutta et al., 1993). Although modeling techniques have been used to examine certain aspects of aeolian transport (e.g., Rasmussen and Sørensen, 2008; Kok et al., 2012; Sullivan and Kok, 2017), those models are still grounded in results from laboratory experiments, and models have not been able to predict the effects of aeolian abrasion on sediments. Thus, new developments in the field hinge on laboratory research. Several unresolved questions provide motivation for such future research. For example, the extent to which aeolian transport of different types of sand contributes to dust and silt production is still debated (Bullard et al., 2007; Crouvi et al., 2010; Adams and Soreghan, 2020; Swet et al., 2020). A relatively new topic of inquiry is "mechanical activation," the mineral alteration of sand by mechanical processes, which may play a role in oxidizing magnetite into hematite during saltation (Merrison et al., 2010). Investigations into these and other topics will necessitate the development of well-constrained experimental devices.

Experimental work is particularly necessary to fill major knowledge gaps in our understanding of past and present aeolian processes on Mars. Aeolian processes have been dominant drivers of global landform-scale change on Mars for billions of years and remain active today (e.g., Greeley and Iversen, 1985; Hayward et al., 2007; Bourke et al., 2008; Diniega et al., 2022). However, patterns of survivability, maturation, and dust production of aeolian sediments on Mars are still unknown (e.g., Fenton et al., 2013; Cornwall et al., 2015; Bristow and Moller, 2018). Our knowledge of these patterns from Earth cannot be directly applied to Mars, because sand on modern-day Mars is primarily mafic rather than felsic (e.g., Fenton et al., 2019), is mobilized at different threshold wind speeds compared to on Earth (e.g., Kok et al, 2012), and is subject to minimal chemical weathering (e.g., Diniega et al., 2022). Closing these knowledge gaps for Mars is particularly important because it could improve provenance research on the sand sources and transport pathways for Martian dune fields (Bourke et al., 2010; Grotzinger et al., 2011). Provenance studies often use spectroscopy to look for mineralogical similarities between sands and their potential source rocks (Langevin et al., 2005; Stockstill-Cahill et al., 2008; Tirsch et al., 2011; Massé et al., 2012; Chojnacki et al., 2014; Lapotre et al., 2017; Burr et al., 2022). However, the concept of mineralogical maturity implies that sand mineralogy would change with increased aeolian transport, possibly becoming different from the source rocks. By characterizing the maturation of Martian aeolian sediments, we could anticipate how sands might change with transport, resolving this major uncertainty in sand provenance research (Fenton et al., 2013; Fenton et al., 2019; Olivarius et al., 2022). Regrettably, the small body of previous research on the subject has yielded uncertain predictions on how basaltic aeolian sands evolve on Mars. For example, remote sensing and terrestrial analog field studies have hypothesized or measured the olivine component of sands to be either depleted (Tirsch et al., 2011; Lapotre et al., 2017) or enriched (Mangold et al., 2011) with aeolian transport, and laboratory studies have been inconclusive with respect to olivine (Cornwall et al., 2015). These contradictory findings demonstrate the need for well-controlled laboratory experiments to directly test these hypotheses and create a comprehensive Mars sediment maturity index.

In previous experimental studies addressing aeolian abrasion and dust production, diverse methods have been utilized to simulate aeolian transport on Earth and Mars (Section 2). However, those previously used devices also have a range of limitations, from designs that place practical restrictions on experiments, to uncertainties regarding similitude (how well the conditions of natural aeolian transport are matched). We did not find any existing device that was capable of simulating the effects of long-distance aeolian transport on a well-constrained, retrievable sand sample while achieving similitude of kinetic energy. Therefore, we decided to create a new device that is optimized for such research.

This device is the Sand AbrasioN Device for Aeolian Research (SANDAR), a modified air mill for simulating the mechanical effects of aeolian transport on sand, applicable to Earth and Mars (Section 3). The SANDAR improves on some of the limitations of devices used in previous research and is better suited for sand-sized particles. We quantify that the SANDAR achieves similitude of kinetic energy (Section 4), and we demonstrate that it effectively simulates natural aeolian transport by evaluating microtextures on the surfaces of abraded sand grains (Section 5). By sharing this device, we hope to give researchers the tools to conduct the experiments necessary to understand aeolian transport throughout the Solar System.

2. Previous experimental devices

Previous experiments on aeolian abrasion have used a variety of methods to simulate the effects of aeolian sand transport. Here, we summarize experimental devices from the literature that have been used to study either the evolution of sand grains undergoing aeolian transport or the production of dust due to aeolian transport of sand on either Earth or Mars. We discuss some of the limitations of those devices, and specifically of the modified Bond mill, that motivated us to redesign it and create a new experimental device. A detailed review of these devices is beyond the scope of this paper but is included as Supplementary Material S1.

2.1. Descriptions of experimental devices

Wind tunnels have long been fundamental tools for understanding the mechanics of aeolian sediment transport, and several researchers have modified wind tunnels to allow for the study of the effects of aeolian transport over large distances. Kuenen (1960a) designed a "circuit tunnel" in which eight air blowers propel sand around a narrow, oval-shaped circuit. Similarly, the "circuit tube" consists of a narrow glass tube shaped into a vertical loop; fine sand grains circulate around the loop and collide with a small sand pile opposite an air jet at the end of a straightaway section (Kuenen, 1960a). Kuenen (1960a), after Knight (1924), also developed a wind tunnel with a conveyor belt floor that acts as a treadmill, continually carrying a bed of sand toward an air blower. Other researchers have utilized classic straight, open-circuit wind tunnels to study long-distance transport by periodically pausing the fan and manually redistributing the sediment in the tunnel (Dutta et al., 1993; Swet et al., 2019; Swet et al., 2020).

Experiments on aeolian abrasion and dust production do not necessarily need to replicate the actual motion of saltation (Forsman, 1978). Saltation is the mechanism of transport that causes collisions between sand grains; for sediment maturation studies such as ours, using other methods to recreate those collisions is acceptable. If the energy levels and dynamics of the collisions are similar to those in saltation, then the same physical weathering effects will occur. Many mechanical and/or air-driven experimental devices were designed following this principle. Krinsley et al. (1979) developed the Mars Erosion Device (MED) to simulate aeolian transport on Mars; this device uses a variable-speed paddle wheel to propel loose sand grains at a mounted sand "target" (Krinsley et al., 1979; Krinsley and Leach, 1979; Krinsley and Greeley, 1986; Greeley and Kraft, 2001). Other researchers have used rotating tumbler devices in which ampoules of sediment are sealed—sometimes at specific Mars atmospheric or environmental conditions—and then repeatedly inverted over monthslong experiments (Merrison et al., 2010; Merrison, 2012; Szynkiewicz et al., 2013; Edgar et al., 2024).

Many experimental devices utilize air pressure to generate sand movement within a chamber. In "test tube" devices, a narrow pipe blows air toward the bottom of a tall, cylindrical glass test tube, agitating the sediment sample within. An electrostatic dust trap near the top of the tube collects any generated dust that has been lofted into suspension (Whalley et al., 1987; Smith et al., 1991; Wright et al., 1998; Bullard et al., 2004; Bullard and White, 2005; Mackie et al., 2006; Bullard et al.,

2007; Bristow and Moller, 2018; Bullard et al., 2022). Marshall et al. (2012) developed a novel experimental apparatus consisting of a bulb-shaped wooden circulation chamber; at the bottom, two air jets propel streams of sand grains to collide at 90° angles. As sand grains move toward the top of the chamber, they lose energy, fall back toward the air jets, and are recycled again. Air mill devices, traditionally used to reduce the particle size of granular material for applications in manufacturing and construction (e.g., Chamayou and Dodds, 2007), have also been used for aeolian research. Such devices use jets of pressurized air to circulate grains around cylindrical cavities ("abrasion chambers") with hard, abrasive walls (e.g., Bond, 1951). Forsman (1978) used an adapted Enraf-Nonius Crystal Grinder mill to simulate the aeolian abrasion of Mars analog sediments at different atmospheric pressures. Later, Cornwall et al. (2015) used a modified Bond mill (Nitkiewicz and Sterner, 1988) for research on the aeolian maturation of Mars-analog sediments.

2.2. Discussion of experimental devices

The requirements of any experimental device depend on the specific intended research applications. Our investigation into aeolian experimental devices was motivated by our ongoing research into sediment maturity and sourcing on Mars (Burr et al., 2022; Burr and Finch, 2024; Baker et al., 2025). We are investigating the mineralogical and textural evolution and dust production of Mars analog sediments, with the ultimate goal of developing a Mars sediment maturity index. These research objectives place practical requirements and restrictions on any experimental device, which unfortunately make some of the previously used devices unsuitable (see Supplementary Material S1 for more details). For example, our sediment samples have to be well-constrained so that we can observe the change in grain size distribution of the sediments over time. Such observations would allow us both to compare the aeolian abrasion rates of different sediments and to measure the rates of dust production (material < 63 μm). Thus, we disfavor experimental devices in which sand-sized grains could be inadvertently lost (Kuenen, 1960a). Furthermore, no external contaminating material should be added to the sample; this requirement excludes devices with walls that tend to become eroded, such as glass tumblers (Merrison, 2012; Szynkiewicz et al., 2013). This requirement also excludes devices that involve interactions between mobile "impactor" grains and stationary, mounted "target" grains (Nieter and Krinsley, 1976; Forsman, 1978; Krinsley et al., 1979). In such devices, any material chipped off the target grains would be added to the population of impactors, making it difficult to constrain the mass or grain size distribution of either population.

Another practical requirement for our experiments is that the device must recirculate the sediment sample in order to simulate the effects of long-distance transport. At the same time, all grains in the sample should experience simulated transport at approximately the same rate, without grain size- or mineralogy-dependent sorting, so that different samples, and sands of mixed grain size or composition, are processed equally. While aeolian sorting does occur in natural dune field settings (e.g., Lapotre et al., 2017), we could not guarantee that any preferential processing within an experimental device would mimic the preferences that occur in nature, so we chose to eliminate sorting as a variable. An additional benefit is that the equal processing of all grains also reduces variability, so that random sampling of the grains is more likely to be representative. This requirement disfavors devices like the circuit tube, in which only finer grains circulate while coarser grains form a pile (Kuenen, 1960a); and the test tube devices, in which material tends to self-sort according to grain size and/or density (Bristow and Moller, 2018).

None of the previous experimental devices align perfectly with our research objectives; however, the modified Bond air mill meets some of our highest priorities. Bond mills were initially invented to create fine crystalline spheres for diffraction experiments (Bond, 1951). Nitkiewicz and Sterner (1988) later described a modified Bond mill made of epoxy resin doped with granular silicon carbide, which was more durable and effective for manufacturing spheres. Cornwall et al. (2015) used this modified Bond mill to simulate the aeolian abrasion of Mars-analog sediments. The modified Bond mill meets several key requirements for our experimental device; it retains sand samples without adding additional material, it is recirculating, and it processes all grains equally. However, because it was initially developed for manufacturing crystalline spheres, it has some limitations when applied to aeolian research. The velocity of sand grains in the modified Bond mill is unknown and cannot be measured because the mill walls are opaque. The modified Bond mill is also too small (2-cm-diameter abrasion chamber with 1-mm-diameter air entrance) to accommodate the sediment sample size required for our research (Section 3.1); Cornwall et al. (2015) used just 10 grains at a time. Another limitation is grain size: any particles < 400 μm could escape via the mill's mesh-covered air exit (and, we found, from between the components of the mill device), eliminating most of the relevant grain size range associated with saltating sand on Earth and Mars (~63–500 μm, e.g., Nickling and Neuman, 2009; Ehlmann et al., 2017; Weitz et al., 2022). We tried to make simple changes to the modified Bond mill to address these limitations, including making the mill larger, using a finer mesh, and adding gaskets between the components. However, those changes resulted in higher air pressures within the abrasion chamber, which caused even more sand to escape from between the components of the mill device.

Given the limitations of the existing experimental devices, we decided to develop a novel device that achieved more of our priorities. We based our experimental device on the modified Bond mill, but we made several changes to its design and developed new manufacturing procedures. The resulting device meets the requirements dictated by our research objectives and is better optimized for aeolian research on sand-sized sediments.

3. The Sand AbrasioN Device for Aeolian Research (SANDAR)

3.1. SANDAR description

The Sand AbrasioN Device for Aeolian Research (SANDAR) (Fig. 1) is an air-driven mill inspired by the modified Bond mill (Nitkiewicz and Sterner, 1988; Cornwall et al., 2015). The SANDAR consists of a mill body made of resin doped with granular silicon carbide (SiC), which creates a durable surface for the circular abrasion chamber (Nitkiewicz and Sterner, 1988). Pressurized air enters through an inlet slot tangent to the wall of the abrasion chamber and causes sand to circulate around the chamber (Supplementary Material S1). This process simulates both sand saltation, via grain-to-grain and grain-to-wall collisions, and creep, via rolling of sand around the abrasion chamber. Air exits through a hole in the back plate that is covered in fine mesh to prevent sand-sized grains from escaping. The front of the abrasion chamber is a glass panel, which provides a window to view the experiment and track sand velocities, resulting in well-constrained experimental conditions. The components are separated by silicone gaskets and held together in a "sandwich" by a custom-machined aluminum vise, which prevents the loss of fine sand even against high air pressures (Fig. 2A).

The SANDAR abrasion chamber is both larger (5 cm diameter) and wider (2.5 cm thick) than the previous modified Bond air mill (2 cm diameter, 1 cm thick). To facilitate even airflow across the entire width of this widened abrasion chamber, the SANDAR air inlet is a slot rather than a round hole (Supplementary Material S2). These changes allow the SANDAR to accommodate a much larger sample size: the SANDAR consistently achieves good circulation with at least 3 g of sediment at a time, in contrast to the 10 grains at a time used in the modified Bond mill (Cornwall et al., 2015). A large sample size offers several advantages. First, the SANDAR holds enough sediment that we can periodically extract small (~0.01 g) portions for electron microprobe analysis. Such regular sampling is necessary to observe how the sediment evolves over time because that evolution tends to be nonlinear (e.g., Greeley and Kraft, 2001; Bullard et al., 2004; Cornwall et al., 2015). Second, our

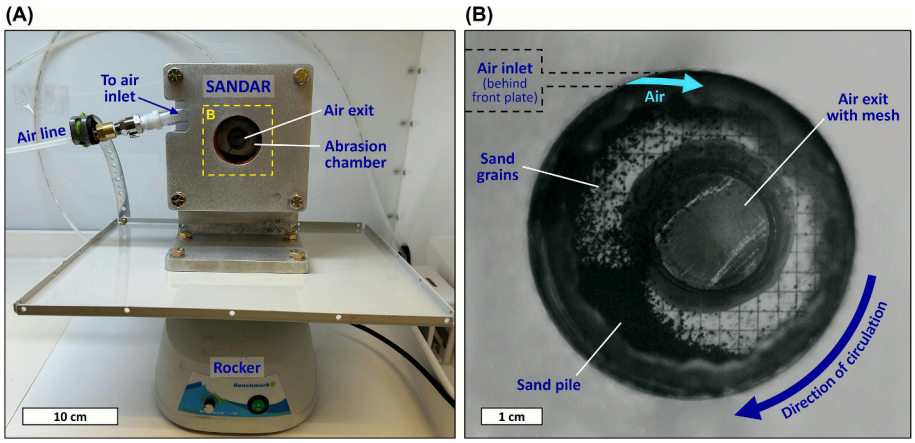

Fig. 1. The Sand AbrasioN Device for Aeolian Research (SANDAR) – (A) Image of the full SANDAR, shown connected to an air line and mounted on a laboratory rocker. Sand is present in the abrasion chamber but is not circulating. (B) High-speed photo of sand circulating in the abrasion chamber of the SANDAR. Air enters through a slot-shaped inlet tangent to the wall of the abrasion chamber and mobilizes the sand. Collisions between circulating sand grains simulate the collisions that occur during aeolian saltation. Air exits through a round hole in the back plate, which is covered by a mesh that keeps sand grains in the abrasion chamber. Sand tends to gather in a pile where airflow is weakest; this pile allows for collisions between circulating sand grains and a bed of loose sediment. During experiments, a rocker (A) tilts the SANDAR slowly back and forth, causing the sand pile to dissipate and re-form, which promotes frequent turnover of grains. The blurry substance visible around the inner circumference of the abrasion chamber is sealant on the glass panel. The sediment shown is 125–500 μm basaltic tephra from Sunset Crater cinder cone in Arizona. Shutter speed is 1/5000. See Supplementary Videos V7, V8, and V9 for regular- and high-speed videos of the sediment and SANDAR in motion.

research is more efficient because we can process a large sample in a single experiment, whereas Cornwall et al. (2015) had to repeat each experiment 10 times to get a sample size of only 100 grains. Third, a large sample size greatly increases the likelihood of grain-to-grain interactions within the abrasion chamber. Grain-to-grain collisions are preferred over grain-to-wall collisions because they better mimic the collisions between sand grains that occur during saltation over beds of loose sediment in natural dune field environments (Forsman, 1978; Bullard et al., 2004; Marshall et al., 2012).

Air exits the mill through a 19.05-mm-diameter hole in the back plate that is covered in a fine mesh (230 × 230 mesh size, 73.66-μm openings, 46 % open area), which holds in sand-sized grains but allows roughly dust-sized particles to escape. This loss of dust simulates the loss of dust to suspension in active dune fields (e.g., Bagnold, 1941). We can still measure dust production rates by measuring the change in mass of the well-constrained sand-sized fraction. The mesh is held in place via compression using an O-ring and short length of pipe with a flange that is bolted to the back side of the back plate (Fig. 2C). The mesh can be removed easily for cleaning or replacement to prevent it from becoming occluded with dust over time, which could inhibit airflow and therefore change air speeds in the abrasion chamber. To prevent sand in the abrasion chamber from collecting around the air exit, the small lip formed by the back plate around the air exit hole is angled slightly inward (toward the front of the mill). The back plate itself is composed of hard coat anodized, sealed aluminum. This surface is resistant to abrasion, and indeed, the back plate shows no signs of abrasion even after ~ 50 h of experiments.

The components of the SANDAR are separated by silicone gaskets and held together in a "sandwich" by four bolts in a custom-machined aluminum vise (Fig. 2A). These design elements allow for tight seals against even the relatively high air pressures that are required to mobilize several grams of sand around a larger abrasion chamber at speeds that match the expected impact velocity of saltating sand on Mars (Section 4.2). Those tight seals, in addition to our changes to the air exit size and mesh, help prevent the inadvertent loss of fine sand. The SANDAR is therefore compatible with grains 74–500 μm, which aligns with the grain size of most saltating aeolian sand on Earth and Mars (e.g., Nickling and Neuman, 2009; Ehlmann et al., 2017; Weitz et al., 2022). Thus, these features help the SANDAR achieve similitude of kinetic energy (Section 4).

During experiments, sand inside the abrasion chamber tends to collect in a small pile under the air inlet slot where the airflow is weakest (Fig. 1B). This sand pile is useful as a source of loose material with which circulating grains can interact, similar to the "dune" in Kuenen's circuit tube (1960a), further increasing the likelihood of grain-to-grain interactions. High-speed video shows that grain collisions with this sand pile effectively induce splashing, an important process in aeolian transport in which the impact of a saltating particle into a bed of sand grains causes those stationary grains to be mobilized (e.g., Beladjine et al., 2007) (Supplementary Video V7). However, any grains that stay in the pile for extended periods would not be abraded as much as circulating grains, which could result in unequal processing of the sample (Kuenen, 1960a). To avoid this potential problem, the SANDAR mill is mounted onto a laboratory rocker (Fig. 1A) that slowly tilts the experimental device back and forth in a seesaw motion ±~20° approximately 2.4 times a minute (Supplementary Video V9). The rocking causes the regular dissipation and re-formation of the sand pile toward the front and then the back sides of the mill in turn, which promotes frequent turnover of grains.

Sand also tends to cling to the walls of the abrasion chamber due to static electricity generated by repeated contacts between sand grains, known as the triboelectric effect (e.g., Forward et al., 2009). To discourage this electrical charging, we treat all surfaces with isopropanol- or bis-hydroxyethyl cocomonium nitrate-based anti-static solution before adding sand and between each timestep of the experiments. Furthermore, the use of the rocker helps prevent any one grain from being stationary for a long period of time by forcing the frequent turnover of sand grains stuck to the front or back panels.

The transparent glass panel provides a view of sand circulating in the abrasion chamber, allowing us to use high-speed photography to observe particle motions, determine modes of abrasion, and measure grain velocities (Supplementary Video V7). This feature allows for consistent, well-constrained experimental conditions because we can ensure that grain velocities match those expected for natural saltating sand and can monitor experiments for interruptions or issues. Additionally, we can change the grain velocity by adjusting the rate of air flowing into the abrasion chamber, the size of the air exit hole, or the characteristics of the air exit mesh. This adaptability makes the SANDAR a versatile instrument that can be used for diverse research applications.

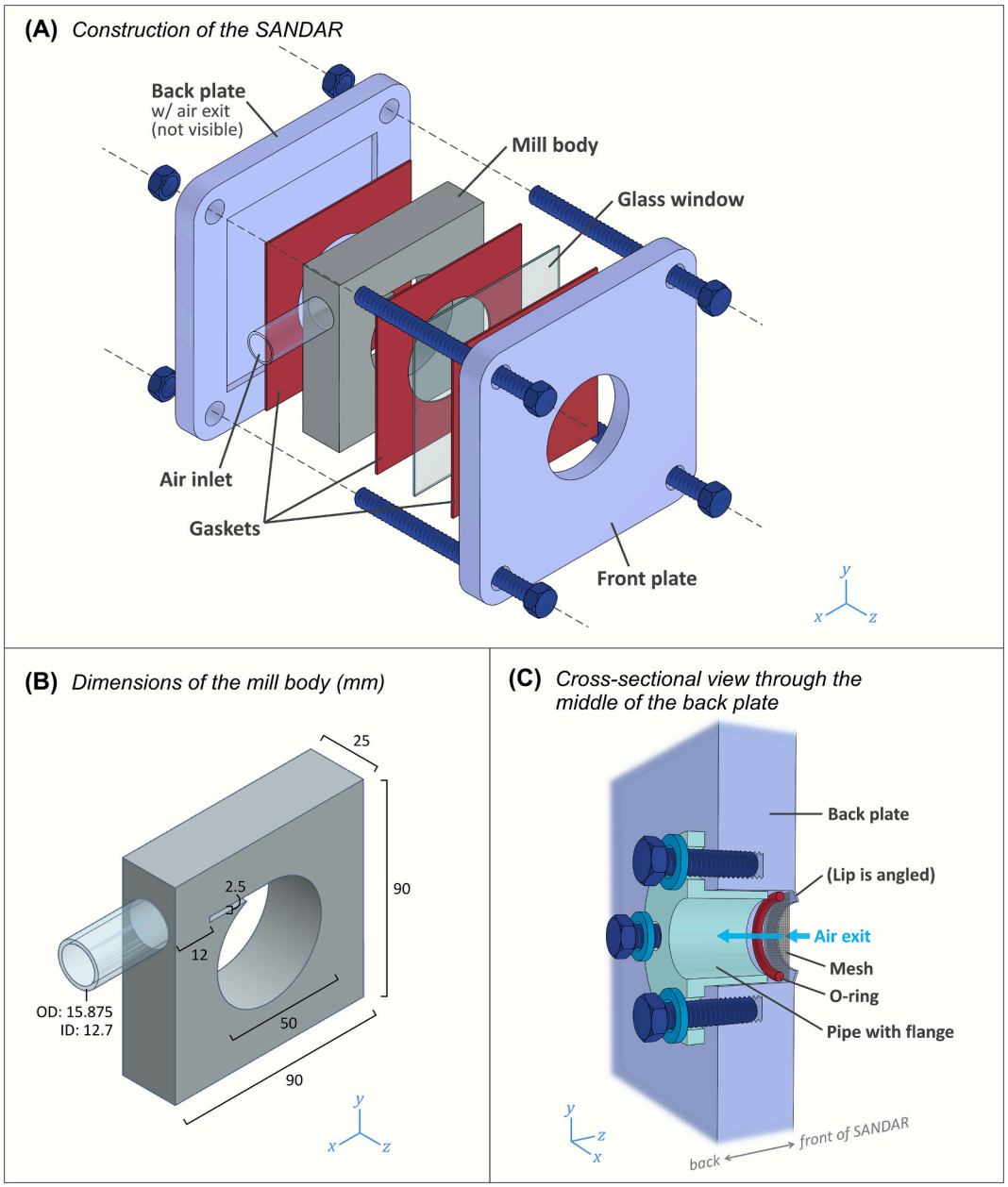

Fig. 2. The components and construction of the SANDAR – (A) Diagram of the SANDAR. The mill body is made of granular silicon carbide mixed with resin. The front and back plates are made of anodized aluminum, and the gaskets are silicone. The bolts are used to hold the SANDAR together and mount it on the rocker platform (not shown). (B) Dimensions of the mill body and air inlet tube, in mm. OD = outer diameter; ID = inner diameter. See Supplementary Material S2 for details on the construction of the mill body. (C) A cross-sectional view of the back plate showing the construction of the air exit. The mesh prevents sand from escaping but allows air and dust-sized grains to exit (blue arrows). The mesh is held in place by compression via an O-ring and a short section of flanged pipe that is screwed into the back plate. The angled lip surrounding the air exit hole prevents sand from collecting around the air exit.

3.2. Mill body

The central component of the SANDAR is the mill body (Fig. 2B; Supplementary Material S2), which is made of a mixture of polyester resin and hard granular silicon carbide (SiC) "grit," modeled after the modified Bond mill (Nitkiewicz and Sterner, 1988). In designing the mill body, we identified three priorities. (1) The mill bodies should have a consistent, uniform, and reproducible composition to ensure that experimental conditions are consistent for each sediment sample. (2) The abrasion chamber walls should be smooth, because any irregularities could cause excess abrasion, provide hollows in which sand could collect, allow pieces of SiC or resin to break off and contaminate the sediment sample, or disrupt the steady, even flow of air around the abrasion chamber. (3) The mill body should be composed of a material that is durable and resistant to abrasion; abrasion of the mill body would be problematic because it would limit the longevity of each mill and because eroded mill material would contaminate the sediment sample. These goals mark a notable deviation from the modified Bond mill (Nitkiewicz and Sterner, 1988), which was designed so that the SiC grit could be easily dislodged from the resin in order to minimize damage to crystal spheres during impacts with the abrasion chamber surface. We experimented with different SiC-to-resin ratios and different procedures for manufacturing the mill body until we identified the best practices for supporting our design priorities (see Supplementary Material S2 for details).

We make the mill bodies by mixing granular SiC (grain size 254 μm)

with Bondo® Liquid Resin for Fiberglass in a 2.1:1 mass ratio. We transfer the mixed slurry to a 3D-printed mold and repeatedly degas it in a vacuum chamber to force out air bubbles. After the mill body has cured, we remove it from the mold and shape the air inlet using diamond coated tools. We cement the inlet tube in place using a resin-and-SiC mix as a glue and filler. Finally, we sand the faces of the mill body smooth to ensure the assembled SANDAR will have tight seals between all components.

The mill bodies held up well during experiments: inspection showed minimal change in the texture of the abrasion chamber walls of a single mill body over ~ 50 h of experiments with various sediments including quartz and basalt (Section 5). We regularly examined portions of the sediment samples under an optical microscope and saw no eroded SiC grains or resin material mixed in. These findings indicate that the mill body provides well-constrained sediment samples and consistent abrasion conditions over our experimental timeframe.

3.3. Limitations of the SANDAR

The SANDAR is designed to be applicable for aeolian research related to either Earth or Mars, and it effectively simulates the most important aspects of aeolian transport for abrasion studies (Section 4). However, the SANDAR does not simulate the atmospheric pressure and temperature of the Martian surface. Simulating low atmospheric pressure was impossible for this air-pressure-driven device, and simulating Mars temperatures would have been both expensive and impractical for experiments that involve the frequent extraction of samples for measurements. Previous studies have shown that environmental conditions have only minimal effects on aeolian abrasion rates. Under low atmospheric pressures, with all other conditions constant, abrasion rates may be slightly increased, likely due to reduced atmospheric "cushioning" (Forsman, 1978; Krinsley et al., 1979). However, these effects are minor: Krinsley et al. (1979) found that quartz sand abraded at Mars pressures compared to Earth pressures had the same rates of change in grain size, only slightly faster rates of grain rounding, and displayed the same types of surface textures, indicating the same mode of mechanical weathering. Lower temperatures are associated with slightly slower abrasion and dust production rates, but the effect of temperature is minor compared to that of other factors like mineralogy and grain velocity (Edgar et al., 2024). There is precedent for conducting similar Mars abrasion experiments at ambient pressure and temperature (e.g., Bullard et al., 2004; Cornwall et al., 2015; Bristow and Moller, 2018).

Grain-to-grain collisions are preferable over grain-to-wall collisions because they better mimic the grain interactions that occur in natural aeolian dune fields (Section 3.1). Collisions with unyielding chamber walls put higher forces on the impacting grains compared to collisions with beds of loose sand; thus, grain-to-wall collisions could cause artificially faster abrasion rates (Bullard et al., 2004; Marshall et al., 2012). Although grain-to-wall collisions do occur in the SANDAR (Supplementary Video V7), as they do in other abrasion and dust production devices (e.g., Kuenen, 1960a; Krinsley et al., 1979; Dutta et al., 1993; Whalley et al., 1987; Bullard et al., 2004; Merrison et al., 2010; Cornwall et al., 2015), we took measures to reduce their frequency, by increasing the size of the abrasion chamber, using much larger sediment samples, and maintaining a pile of stationary loose sediment. Another mitigating factor is that those grain-to-wall impacts often occur at low angles due to the circular shape of the abrasion chamber, resulting in less potential for abrasion (White et al., 2006; Marshall et al., 2012).

Correlating abrasion time in the SANDAR with the equivalent distance of real-world aeolian transport would allow us to use our sediment survivability findings to place quantitative bounds on the scale of aeolian transport. However, such correlations are difficult to determine, particularly for Mars (e.g., Rogers and Christensen, 2003), where many parameters for aeolian transport are still uncertain. Future efforts to establish such a correlation could involve estimating grain collision rates from high-speed video or comparing SANDAR-abraded sediments to sediments that have been transported known distances in dune fields or wind tunnels.

These limitations do not affect our ability to use the SANDAR to compare the relative abrasion and dust production rates of different minerals and sediment types, provided that experimental conditions are held constant. Such relative comparisons are sufficient for many research objectives (e.g., Bullard et al., 2004), including determining a sediment maturity index.

4. Similitude

4.1. Similitude parameters

For aeolian abrasion and dust production experiments, we posit that the kinetic energy of impacting sand grains (E_k) is the most important similitude parameter to match to natural, real-world aeolian processes (Marshall et al., 2021). The kinetic energy of an impacting particle is directly proportional to susceptibility to abrasion, or the amount of mass that is removed by the impact (Greeley et al., 1982; Greeley and Iversen, 1985; Anderson, 1986). Kinetic energy determines what mode of abrasion occurs (Krinsley et al., 1979), which microtextures form on the surfaces of sand grains (Marshall et al., 2012), and ultimately whether those grains can be fractured on impact (Dutta et al., 1993; O'Hara-Dhand et al., 2010). Kinetic energy depends on the mass (m) of sand grains—which can be determined from their diameter (D_p) and density (ρ), assuming spherical grains—and on their impacting velocity (v_{imp}) (e.g., Rumpel, 1985; Dutta et al., 1993):

$$E_k = \frac{1}{2} m v_{imp}^2 = \frac{1}{2}\left(\rho \frac{4\pi}{3}\left(\frac{D_p}{2}\right)^3\right) v_{imp}^2 \quad (1)$$

The velocities of saltating particles vary throughout their trajectories; the impact velocity describes the speed of a particle just before it collides with the bed surface, which occurs when the height above the bed is zero (e.g., Kok et al., 2012; O'Brien and McKenna Neuman, 2016). Particle impact velocity is affected by factors including the wind velocity gradient, the fluid properties of the air, and the trajectories of saltating sand grains (Bagnold, 1941; Greeley et al., 1982; Greeley and Iversen, 1985; Zou et al., 2001; Kok et al., 2012; Zheng et al., 2013; Sullivan and Kok, 2017).

In addition to matching the overall kinetic energy, whenever possible, we also try to directly match the specific grain sizes and particle velocities to those in natural aeolian environments. These variables may help promote further similitude because grain size helps determine the mechanical durability of particles (e.g., Brecker, 1974)—the cross-sectional area of a grain is proportional to the bond energy that must be exceeded for the grain to fracture (Dutta et al., 1993). Grain size and particle velocity may also be particularly relevant for certain research objectives. For example, grain size determines the surface-to-volume ratio, which is important for investigations into dust production by abrasion of sand grains with mineral coatings (e.g., Swet et al., 2019).

Another parameter that has been used as the basis for similitude in particle collision experiments is the Froude number (Fr) (Rasmussen et al. 2015), a dimensionless parameter that describes the characteristics of fluid flow due to the forces of inertia and gravity. Rasmussen et al. (2015) define the Froude number for particle collision experiments as $Fr = v_{imp}/\sqrt{gD_p}$, where g is acceleration due to gravity; thus, like kinetic energy, the Froude number depends on impacting particle velocity and diameter. We prefer kinetic energy as the similitude parameter because it has been directly linked to susceptibility to abrasion (Greeley et al. 1982; Greeley and Iversen 1985; Anderson 1986) and because it accounts for particle density.

Because our research is focused on aeolian abrasion and dust production rather than sand transport dynamics, several parameters that are important for some wind tunnel experiments are not relevant here (Marshall et al., 2021). The SANDAR does not simulate saltation

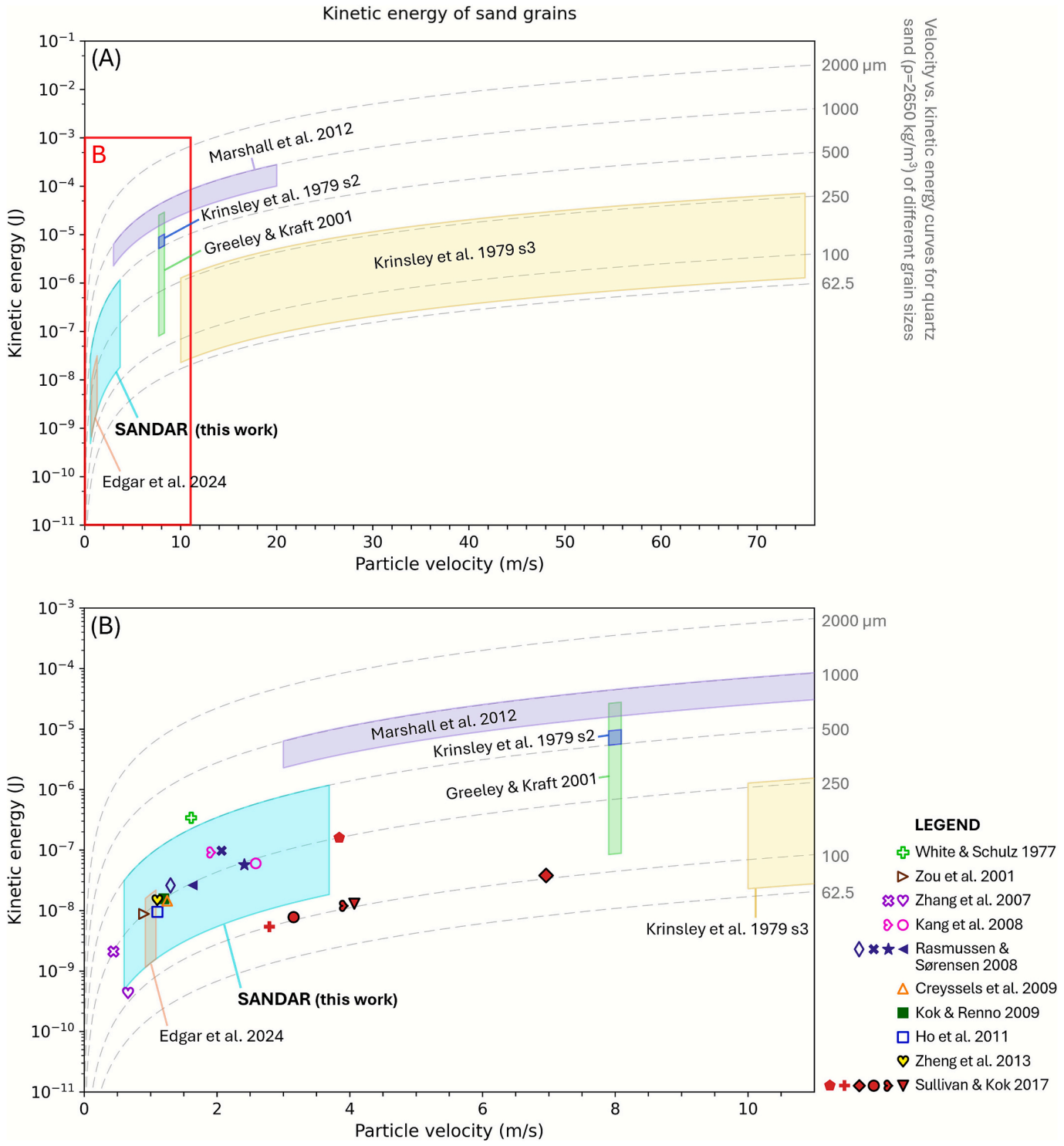

Fig. 3. Kinetic energy of saltating sand grains – Kinetic energy of sand grains in abrasion experiments (shaded regions) and in natural saltation (points). Figure (B) shows in detail the area outlined in red in (A). The dashed gray lines represent kinetic energy versus velocity curves for quartz sand (density = 2650 kg/m^3) of various grain sizes, included here for context. The cyan region shows the energy regime of sediment in the SANDAR (grain size = 125–500 µm, density = 2650 kg/m^3, this work); other shaded regions show the energy regimes of sediment in different aeolian abrasion experiments from the literature. The regions labeled "Krinsley et al. 1979 s2" and "Krinsley et al. 1979 s3" refer to stages 2 and 3 of the Krinsley et al. 1979 study, respectively. Points represent typical impact velocities and kinetic energies of saltating sand on Earth or Mars according to the literature. Open point markers are from wind tunnel studies, filled markers are from modeling studies, and markers with black outlines are from modeling studies using Mars conditions. Tables 1 and 2 describe the experimental conditions associated with each of the points and regions, respectively.

trajectories, so it is not necessary to achieve similitude with parameters affecting the trajectories of particles, such as the fluid viscosity and the particle Reynolds number. Similarly, we are not investigating the initiation of particle motion; thus, values like Shields parameter are not considered.

4.2. Kinetic energy of natural saltating sand

To identify our target kinetic energy, we reviewed the literature for examples of expected impact kinetic energy values for natural saltating sand, represented as points on Fig. 3. These data come from both wind tunnel experiments (White and Schulz, 1977; Zou et al., 2001; Zhang et al., 2007; Kang et al., 2008; Rasmussen and Sørensen, 2008; Creyssels et al., 2009; Ho et al., 2011) and modeling studies (Rasmussen and Sørensen, 2008; Kok and Renno, 2009; Zheng et al., 2013; Sullivan and Kok, 2017) conducted with various sediment types and wind conditions and set on either Earth or Mars (Table 1). For visual clarity, we only included a few representative data points from each reference, because other points either overlap or plot nearby. We used the reported impact velocities to calculate kinetic energy (or vice versa) according to Equation (1), assuming spherical grains. For studies that did not directly measure or extrapolate the impact velocity—which occurs at height above the bed (z) = 0—we used the velocity at the smallest z for which data were given. Several of the studies did not discriminate between ascending and descending grains (only descending grains are relevant for the impact velocity). Ascending grains tend to have slightly lower

Table 1
Velocity and kinetic energy of natural saltating sand according to the literature.

Reference	Symbol on Fig. 3	Study type	Particle density (kg/m^3)	Particle diameter (μm)	Wind velocity u_* or U_0 (m/s)	Particle impact velocity (m/s)	Particle kinetic energy (J)
EARTH:							
White & Schulz, 1977	✚	WT	2500	586	$u_* = 0.396$	1.612	3.42×10^{-7}
Zou et al., 2001	▷	WT	2650[†]	250	$u_* = 0.81$	0.9[a]	8.78×10^{-9}
Zhang et al., 2007	♡	WT	2700	112	$U_0 = 6.5$	0.66 [a]	4.33×10^{-10}
Zhang et al., 2007	⊠	WT	2650	250	$U_0 = 8.05$	0.44 [a]	2.10×10^{-9}
Kang et al., 2008	○	WT	2650[‡]	235	$U_0 = 10.9$	2.58	6.01×10^{-8}
Kang et al., 2008	◗	WT	2650[‡]	330	$U_0 = 16.2$	1.91	9.13×10^{-8}
Rasmussen & Sørensen, 2008	◇	WT	2650[‡]	281	$u_* = 0.27$–0.74[#]	1.3[a,b]	2.60×10^{-8}
Rasmussen & Sørensen, 2008	◀	Model	2650[‡]	242	$u_* = 0.27$	1.63[a,b]	2.61×10^{-8}
Rasmussen & Sørensen, 2008	★	Model	2650[‡]	242	$u_* = 0.69$	2.41[a,b]	5.71×10^{-8}
Rasmussen & Sørensen, 2008	✖	Model	2650[‡]	320	$u_* = 0.74$	2.07[a,b]	9.74×10^{-8}
Creyssels et al., 2009	△	WT	2500	242	$u_* = 0.48$	1.25[a,b]	1.45×10^{-8}
Kok & Renno, 2009	■	Model	2650	250	$u_* = 0.2$–1.0[#,¶]	1.2	1.56×10^{-8}
Ho et al., 2011	□	WT	2470	230	$u_* = 0.44$–1.0[#]	1.10[a,b]	9.52×10^{-9}
Sullivan & Kok, 2017	⬟	Model	2650	250	$u_* = 0.3$	3.84	1.6×10^{-7}
Sullivan & Kok, 2017	✚	Model	2650	100	$u_* = 0.3$	2.79	5.4×10^{-9}
MARS:							
Zheng et al., 2013	♡	Model	3000	250[§]	$u_* = 0.5$[c]	1.10	1.48×10^{-8}
Sullivan & Kok, 2017	◆	Model	3000	100	$u_* = 0.5$[c,††]	6.96	3.8×10^{-8}
Sullivan & Kok, 2017	●	Model	3000	100	$u_* = 0.5$[c]	3.15	7.8×10^{-9}
Sullivan & Kok, 2017	◗	Model	3000	100	$u_* = 1.0$	3.91	1.2×10^{-8}
Sullivan & Kok, 2017	▼	Model	3000	100	$u_* = 2.0$	4.07	1.3×10^{-8}

NOTES: WT = Wind tunnel. Unless otherwise stated: the particle impact velocity includes only descending grains; the particle impact velocity includes both horizontal and vertical components; the wind speed was above the fluid threshold ($u_* > u_{*tf}$). [a]Includes both ascending and descending grains. [b]Includes horizontal velocity only. [c]Wind energy regime: $u_{*ti} < u_* < u_{*tf}$. [†]Particle density was not reported and so is assumed based on the composition. [‡]Neither particle density nor composition were reported; density is assumed to be that of typical terrestrial quartz sand. [§]Velocity was calculated from an equation that did not include grain size, but 250 μm was used as an example in the paper. [#]Found that impact velocities converged independent of u_*. [¶]u_* values were reported in Kok et al., 2012, Fig. 14D. [††]Model did not include the effects of a saltation cloud on wind profile.

speeds than descending grains at the same height z (e.g., Kang et al., 2008), so for those studies, the reported average velocity at $z = 0$ may underestimate the impact velocity. Additionally, some studies only reported the horizontal component of the velocity (the vertical component tends to be minor, e.g., Kang et al., 2008), which may also result in slight underestimates. These estimates can still be relevant and useful; for example, Rasmussen and Sørensen (2008) looked at the horizontal velocities of combined ascending and descending grains and found that their measured and modeled velocities were still within the lower end of the range expected for impact velocities.

Table 1 also describes the sediment grain size and experiment or model conditions for each of the points on Fig. 3. All experiments and models involved the transport of sand over beds of loose, erodible sediment. Wind conditions are reported in terms of either the free stream wind velocity (U_0) or the wind friction velocity (u_*). All the Earth-based experiments and models were conducted at conditions such that u_* was above the fluid threshold (u_{*tf}), which is the minimum wind friction velocity required to initiate saltation due to wind energy alone. In contrast, several of the Mars-based modeling studies (Zheng et al., 2013; Sullivan and Kok, 2017) used wind speeds *below* the fluid threshold and above the impact threshold (u_{*ti}), which is the wind friction velocity required to sustain saltation after it has already begun. The impact threshold is lower than the fluid threshold due to the impact energy imparted by collisions with already-saltating grains (Bagnold, 1941). Much of sand transport on Mars is believed to occur below the fluid threshold (Kok, 2010; Kok et al., 2012; Sullivan and Kok, 2017; Swann et al., 2020; Andreotti et al., 2021). Supplementary Table S3 provides additional details on the experimental conditions, methods, and assumptions associated with each kinetic energy value.

Table 1 – Velocity and kinetic energy values for natural saltating sand on Earth and Mars according to wind tunnel and modeling studies. Each item corresponds to a point on Fig. 3. For experiments involving a range of grain sizes, the mean or median grain size (if reported) or the middle value of the range was used here. The wind conditions are reported in terms of either the friction velocity (u_*) or the free-stream wind velocity (U_0). Particle impacting velocities were measured at or extrapolated to either $z = 0$ or the smallest possible z for which data were given. See Supplementary Table S3 for more information on experimental conditions.

4.3. SANDAR similitude experiment

As we developed the SANDAR, we measured the kinetic energy of particles circulating in the abrasion chamber to evaluate its similitude. For these tests, we used ~ 2 g of sand from Sunset Crater, a young basaltic cinder cone in the San Francisco Volcanic Field in northern Arizona (Hooper et al., 2012; Alfano et al., 2019). The Sunset Crater sand has a density of about 2650 kg/m^3. We sieved the sand to isolate the 125–500 μm grain size fraction, which is a typical grain size range for saltating sediment on Earth and Mars (e.g., Nickling and Neuman, 2009; Weitz et al., 2022; Burr et al., 2024).

We used high-speed photography to measure the velocities of grains circulating in the abrasion chamber. We filmed circulating sand grains at 2500 frames per second with shutter speed 1/5000 using an Edgertronic video camera (Supplementary Video V7). We measured particle velocities from the footage using both the Manual Tracking and TrackMate (Ershov et al., 2022) plugins on ImageJ/Fiji (Schindelin et al., 2012). Sand grains in different parts of the abrasion chamber tend to have different velocities, and many grains are either hidden behind overlapping grains or stationary (in the "sand pile") at any given time, so we could not take a representative sample of velocities to find the mean. Instead, we tracked a selection of particularly slow and fast grains to get a sense of the distribution of velocities of particles in the SANDAR.

Through a series of trial-and-error experiments, we found that we achieved the highest degree of similitude using the SANDAR size and geometry described in Section 3 and an airflow into the SANDAR of 1.6 standard cubic feet per minute (0.045 m^3/min), which corresponded to a pressure of ~ 60 psi (4.1 bar) in the air line. Using that setup, most tracked grains had impacting velocities of 0.6–3.7 m/s. From Equation (1), this range corresponds to kinetic energies between 4.88×10^{-10} and 1.19×10^{-6} J (Fig. 3).

4.4. Discussion of similitude

The kinetic energies of particles in the SANDAR are similar to those expected of saltating sand in natural aeolian settings on Earth and Mars according to the literature (Fig. 3). Most particles in the SANDAR have kinetic energies between 4.88×10^{-10} and 1.19×10^{-6} J, and the modeled and measured kinetic energy values from the literature have a similar range, from a minimum of 4.33×10^{-10} J (Zhang et al., 2007) to a maximum of 3.42×10^{-7} J (White and Schulz, 1977). Furthermore, our SANDAR setup also has particle velocities (represented by the x-axis on Fig. 3) and particle sizes and densities (represented by the dashed curved lines) similar to natural sand in saltation. The range of particle velocities in the SANDAR (0.6–3.7 m/s) closely matches the range of modeled and measured particle impact velocities for saltating sand on Earth, the minimum of which is 0.44 m/s (Zhang et al., 2007) and the maximum of which is 3.84 m/s (Sullivan and Kok, 2017). Even the higher particle impact velocities thought to be associated with aeolian transport on Mars are fairly well represented. Most of the modeled impact velocities listed here for saltating sand grains on Mars range from 1.10 m/s (Zheng et al., 2013) to 4.07 m/s (Sullivan and Kok, 2017), including those from experiments at high wind friction speeds (u_*=1.0 and 2.0 m/s) well above the fluid threshold. However, impact velocities are higher for Mars models involving sporadic grain motion rather than saltation within a cloud of saltating particles—under those conditions, at u_*=0.5, modeled impact velocity is 6.96 m/s (Sullivan and Kok, 2017). Even in that case, the kinetic energy (3.8×10^{-8} J) is well within the range of the SANDAR. Thus, we conclude that the SANDAR achieves similitude of kinetic energy for aeolian transport on both Earth and Mars.

For context, we also compared kinetic energy in the SANDAR to other experimental devices that have been used in the literature to simulate aeolian abrasion on Earth and Mars. The shaded regions in Fig. 3 show the energy regimes of other experimental studies that reported grain velocities; the grain velocity metric was necessary to calculate kinetic energy using Equation (1). Those studies used a variety of experimental devices: the Mars Erosion Device (Krinsley et al., 1979; Greeley and Kraft, 2001), the Marshall apparatus (Marshall et al., 2012), and rotating tumblers kept at Mars atmospheric pressures and temperatures (Edgar et al., 2024). The experimental conditions and other specifications for each of those experiments are described in Table 2; see Supplementary Table S4 for additional details. Of the experimental devices compared, the SANDAR provides the closest match for typical kinetic energies and velocities of natural saltating sand on both Earth and Mars, sometimes by several orders of magnitude (Fig. 3). The tumbler

Table 2
Velocity and kinetic energy of sand in aeolian abrasion experiments.

Reference	Experimental device	Planet of interest	Particle density (kg/m^3)	Initial particle diameter range (μm)	Particle impact velocity (m/s)	Minimum particle kinetic energy (J)	Maximum particle kinetic energy (J)
Krinsley et al., 1979 stage 2	Mars Erosion Device	Earth	2650[†]	125–850	8	8.67×10^{-8}	2.73×10^{-5}
Krinsley et al., 1979 stage 3	Mars Erosion Device	Mars	1200[‡]	90–344	10–75	2.29×10^{-8}	7.19×10^{-5}
Greeley and Kraft, 2001	Mars Erosion Device	Mars	2650[†]	500–600	8	5.55×10^{-6}	9.59×10^{-6}
Marshall et al., 2012	Marshall apparatus	Earth	2700	710–1000	3–20	2.28×10^{-6}	2.83×10^{-4}
Edgar et al., 2024	Tumbler	Mars	2650[†]	125–300	1	1.36×10^{-9}	1.87×10^{-8}
This work	SANDAR	Earth & Mars	2650	125–500	0.6–3.7	4.88×10^{-10}	1.19×10^{-6}

NOTES: [†]Particle density was not reported and so is assumed based on the composition. [‡]Particle density was described only as "similar to pumice," which is typically ~ 700–1200 kg/m^3 (e.g., Shipley and Sarna-Wojcicki, 1983).

devices used by Edgar et al. (2024) to simulate aeolian abrasion on Mars have a reported kinetic energy and velocity regime that overlaps with that of the SANDAR, but is more limited, with kinetic energy not exceeding 1.87×10^{-8} J based on an estimated grain impact velocity of ~ 1 m/s (Merrison, 2012). That impact velocity would be consistent with the low end of the range of expected impact velocities for saltating sand on Earth, but slower than most expectations for impact velocities on Mars (Section 4.2). Furthermore, the velocity of particles in the tumblers was not directly measured; instead, it was estimated theoretically from gravitational acceleration and the length of the tumbling ampoules (Merrison, 2012). This estimate assumes that particles are in freefall for the entire length of the ampoule, ending in ballistic impacts; however, we question that assumption based on studies of the movement of granular material in rotating circular drums (Henein et al., 1983; Stanev et al., 2014). In a circular drum with diameter equal to the length of the ampoule and rotating at the same rate, the particles would have a rotational Froude number of 0.0023, which typically results in slumping motion (Stanev et al., 2014). Thus, of the examined experimental devices, the SANDAR provides the greatest likelihood of achieving similitude of kinetic energy.

Table 2 – Velocity and kinetic energy levels for sand in aeolian abrasion experiments from the literature. Each item corresponds to a shaded region in Fig. 3. The experimental devices are described in detail in Section 2.1. Note that kinetic energies were calculated using the initial grain size ranges of sand particles in the experiments; for some experiments, grain size may have decreased over time as sand grains were comminuted. See Supplementary Table S4 for more information on experimental conditions.

Although we prefer kinetic energy as a similitude parameter, we also calculated the Froude number for material in the SANDAR to ensure that was also consistent with natural conditions. Particles 125–500 μm in the SANDAR had velocities between 0.6–3.7 m/s, corresponding to Froude numbers of ~ 10–100. Rasmussen et al. (2015) report that saltating sand on Earth with grain size 200 μm typically has impacting velocities of 1 to 5 m/s, corresponding to Froude numbers of ~ 20–100. Thus, the Froude numbers for particles in the SANDAR also align closely with those in natural settings.

Our measurements demonstrate that the SANDAR is capable of simulating typical aeolian saltation on Earth and Mars—but crucially, it is not limited to those conditions. The SANDAR can also be used to achieve other kinetic energies by changing the size or density of the sand grains and the rate of air flowing into or out of the abrasion chamber. This versatility means that the SANDAR can be adapted for research on extreme wind environments, unusual sediment types, and potentially even aeolian transport on other planetary bodies like Venus or Titan.

5. Validation of Method

To evaluate whether the SANDAR effectively recreates the specific mechanical effects of aeolian transport on sand grains, we examined sediment abraded in the SANDAR for microtextures known to be associated with natural aeolian transport. Microtextures are micrometer-scale surface features on sediment grains caused by mechanical or chemical alteration during weathering, transport, or diagenesis of the sediment (e.g., Krinsley and Takahashi, 1962). Different modes of sediment transport involve different mechanical processes and energy levels and so result in different microtextures; these microtextures have been studied extensively through both experiments and observation of natural sediments (e.g., Krinsley and Donahue, 1968; Krinsley and Doornkamp, 1973; Mahaney, 2002; Costa et al., 2012; Marshall et al., 2012; Vos et al., 2014; Costa et al., 2017). If sand grains abraded in the SANDAR show microtextures and morphologies diagnostic of aeolian transport, it would indicate that the SANDAR accurately simulates the mechanical effects of saltation, validating the use of the SANDAR in aeolian research (Krinsley et al., 1979).

5.1. *Quartz microtextures experiment*

We chose to use quartz sand for our first microtexture validation experiment because the morphological and microtextural effects of different modes of transport on quartz sand grains have been well studied (Knight, 1924; Kuenen, 1960b; Kuenen, 1962; Krinsley and Doornkamp, 1973; Whalley et al., 1987; Costa et al., 2012; Costa et al., 2013; Vos et al., 2014). We used a rock hammer and mortar and pestle to crush a milky quartz specimen obtained through Ward's Science from a vein in the Coso Range, Inyo County, California. We sieved the crushed fragments to isolate the 250–500 μm grain size fraction typical of saltating dune sands on Earth. We abraded a 3-g sample of this crushed quartz in the SANDAR for 33.85 h total, stopping every few hours to take representative samples for analysis and sieve out and remove the dust (<63 μm). We replaced the air exit mesh halfway through this

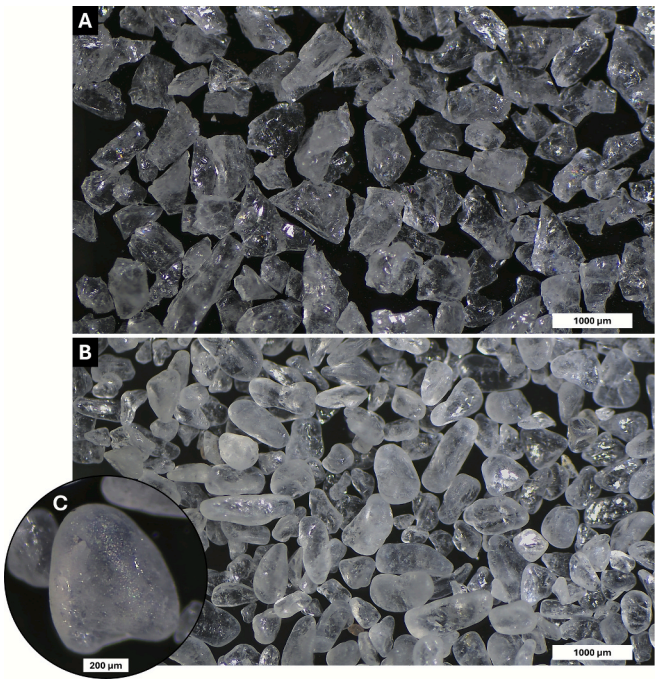

Fig. 4. Optical microscope images of quartz sand before and after abrasion in the SANDAR – (A) Freshly crushed quartz grains were highly angular, with sharp edges and smooth, reflective surfaces. (B) After 33.85 h of abrasion in the SANDAR, quartz grains were subrounded to well rounded. Many grains also show frosting, evidenced by their slight opacity, due to repeated mechanical collisions. These characteristics are associated with aeolian transport. (C) A closeup image of a frosted quartz grain after 9 h abrasion in the SANDAR shows the low-relief rough texture on the surface of the grain that causes its frosted appearance. Images were captured under reflected light using a View4K camera on an Olympus SZ61 microscope.

experiment to prevent it from accumulating dust and obstructing airflow. We conducted this experiment using a prototype of our final SANDAR setup, which had a reduced airflow (1.4 standard cubic feet per minute, or 0.04 m^3/min) and finer air exit mesh (50 × 250 mesh size, which filters particles < 60 µm) compared to normal operating conditions. Under these conditions, grain velocities ranged from ~ 0.4 to 2.9 m/s, corresponding to kinetic energies ranging from 1.73×10^{-9} to 7.29×10^{-7} J.

Optical microscope images show that quartz sediment abraded in the SANDAR developed morphologies and characteristics consistent with aeolian transport (Fig. 4). The initial crushed grains were angular, sharp, transparent, and reflective, but they became increasingly rounded and frosted with increased time in the SANDAR. Frosting is a common feature associated with aeolian environments that occurs due to mechanical abrasion during repeated grain-to-grain collisions (e.g., Kuenen, 1962; Margolis, 1974). (In natural aeolian settings, chemical weathering processes can also contribute to frosting, but our experiments only simulate mechanical processes because those are the primary drivers of sediment maturation on modern-day Mars.).

In scanning electron microscope (SEM) secondary electron images, quartz grains abraded in the SANDAR revealed an assemblage of microtextures that is strongly associated with aeolian transport (Fig. 5). All grains examined from the sample abraded for 33.85 h (n≈30) had the rounded outlines, bulbous edges, low relief, and upturned plates that are characteristic of aeolian sediments. Bulbous edges in particular are considered diagnostic of aeolian transport, caused by the rotation of saltating grains (Vos et al., 2014). Other features associated with aeolian transport that were present include elongated depressions (ED), small to medium conchoidal fractures (CF), graded arcs (GA), meandering ridges (MR), crescentic percussion marks (CP), and abrasion fatigue evidenced by the presence of adhering fine particles (Mahaney, 2002; Vos et al., 2014). All the mechanical features identified in a Vos et al. (2014) review paper as "abundant" or "common" in aeolian desert dune settings were present in the SANDAR-abraded sample (Supplementary Table S5). Significantly, there were no features present that are not associated with aeolian settings. This specific assemblage of microtextures points to a uniquely aeolian setting, indicating that the SANDAR effectively recreates the mechanical effects of aeolian transport.

5.2. *Basalt microtextures experiment*

To ensure that the SANDAR would also effectively simulate aeolian transport for Mars-relevant materials (e.g., Fenton et al., 2019), we conducted an additional validation experiment using basaltic sand. The sediment for this experiment was glassy, varnished basaltic tephra with clasts of olivine, plagioclase, and pyroxene from Pisgah Crater, a Mars analog cinder cone in the Mojave Desert, California (Guinness et al., 1997). We sieved the uncrushed sediment to a grain size of 250–500 µm and abraded a 3-g sample in the SANDAR for 12 h using the same experimental conditions described in Section 5.1. We paused the experiment periodically to take small representative samples for analysis and sieve out and remove any dust. We used an SEM to examine the microtextures on grains before, at various stages during, and after abrasion (Fig. 6).

The microtextures that form on basaltic sand due to aeolian transport have not been extensively documented, so rather than referring to the literature, we directly compared the experimental sediment to samples of basaltic sand that have undergone natural aeolian transport in a dune field. We obtained this natural sand from the active Grand Falls dune field in the Navajo Nation in northern Arizona, which has been recognized as a Mars analog dune field because of its basaltic sediment and dry climate (Hayward et al., 2010; Bristow and Moller, 2018; Gullikson et al., 2023). Representatives from the U.S. Geological Survey collected the sand under a permit from the Navajo Nation during the dry, windy season using saltation sediment traps that caught airborne particles up to 9 cm above the bed surface (see Supplementary Material S6 for a map of the sampling location). The sand at Grand Falls dune field is bimodal, containing felsic and basaltic grains. We used an optical microscope to visually inspect grains from the 250–500 µm grain size fraction and isolate the basalt for comparison with the experimental sediment.

Before abrasion, the Pisgah Crater tephra was highly angular, with smooth surfaces and sharp edges (Fig. 6). Abundant vesicles and sharp protrusions formed complex grain shapes. SEM images of the sample after only 120 min of abrasion show fewer protrusions and more rounded edges. Signs of abrasion on only the edges and corners of grains indicates that those sharp features were the first to be affected. This finding is consistent with a geometric theory of abrasion that has been described for fluvial pebbles, which posits that abrasion of blocky particles occurs in two phases: first, protrusions are removed as grains are rounded to smooth, convex shapes; second, grain size is slowly reduced with continued abrasion (Bloore, 1977; Domokos et al., 2014; Miller et al., 2014). After 300 min in the SANDAR, the grains became more rounded and showed signs of abrasion on most surfaces. The morphologies and microtextures of the SANDAR-abraded Pisgah Crater sand were very similar to those of the natural aeolian Grand Falls sand. Both samples had rounded grains with low-relief microtextures giving the appearance of rough surfaces. Abundant small, randomly oriented indents are likely evidence of individual collisions between particles. The similarity between the experimental and natural aeolian samples indicates that the SANDAR effectively simulates the mechanical processes of aeolian transport for sands of compositions other than quartz.

6. Conclusions

Experimental research on the effects of aeolian abrasion on sand grains is essential to advance our understanding of aeolian processes and

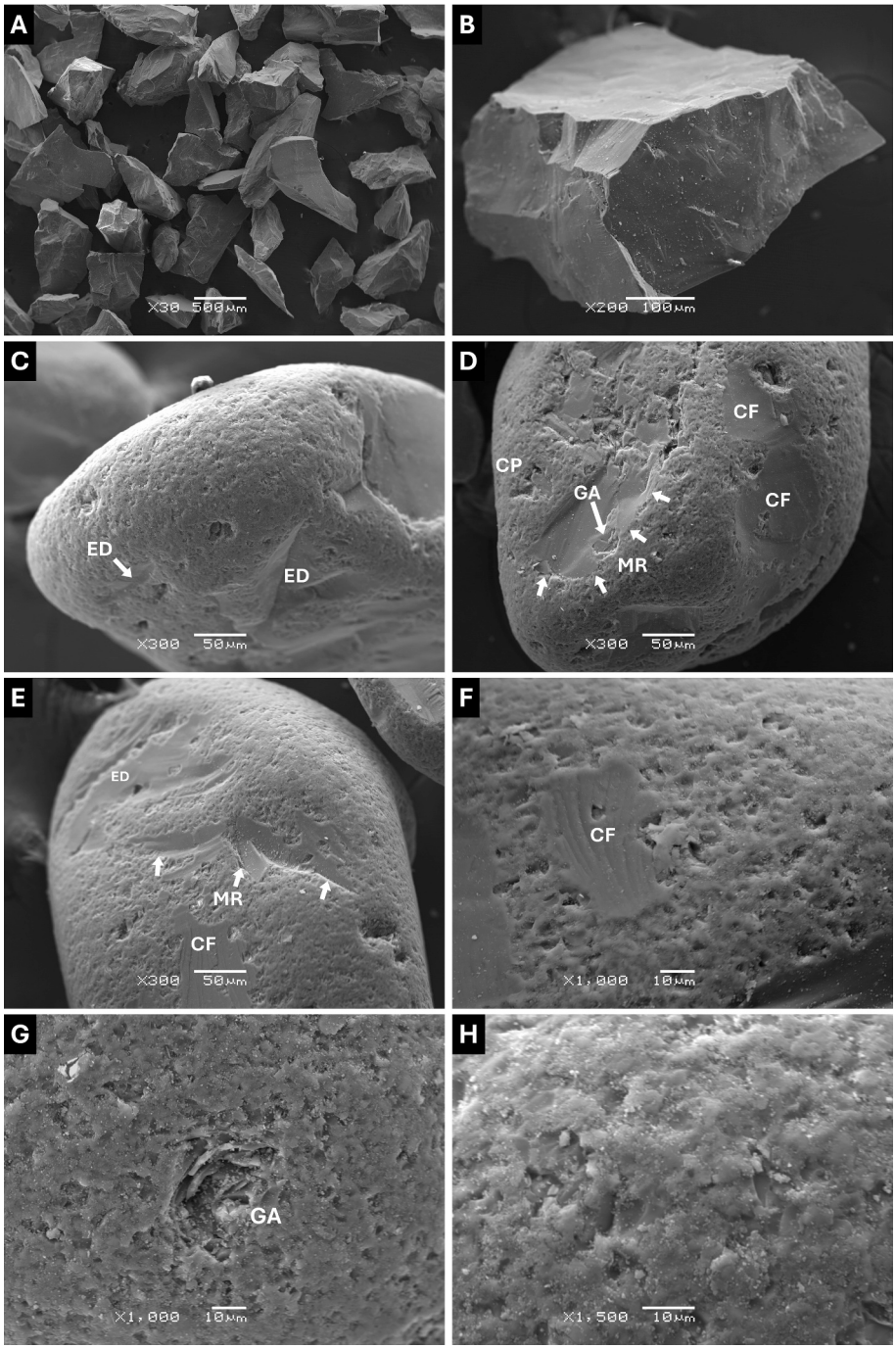

Fig. 5. SEM images of aeolian microtextures on quartz sand – SEM secondary electron images of microtextures on freshly crushed quartz (A and B) and quartz after 33.85 h of abrasion in the SANDAR (C to H). Abraded grains show morphologies and microtextures indicative of aeolian transport. [A and B] Crushed quartz before abrasion in the SANDAR. The crushed quartz grains are highly angular, with sharp edges, smooth surfaces, and some conchoidal fractures. The small particles (<10 µm) are resident fines, byproducts from the crushing process (grains were not washed before imaging). [C] A rounded grain with bulbous edges and several elongated depressions (ED). The surface is covered in upturned plates and has a low- to medium-relief texture. [D] A rounded grain with bulbous edges and conchoidal fractures (CF), graded arcs (GA), and meandering ridges (MR, short arrows). The surrounding surfaces are textured in low relief with crescentic percussion marks (CP) and upturned plates. [E] A rounded grain with several meandering ridges (MR, arrows) and elongated depressions (ED). The bottom of the image shows a conchoidal fracture (CF) with straight steps. The rest of the grain is covered in low-relief upturned plates. [F] A medium-sized conchoidal fracture (CF) with arcuate steps surrounded by upturned plates. Conchoidal fractures can also be found on the initial crushed quartz (B), but the fact that this conchoidal fracture overlies an abraded surface indicates that it formed in the SANDAR. Resident fine particles adhering to the grain are evidence of abrasion fatigue. [G] A graded arc (GA) surrounded by upturned plates. Adhering particles are evidence of abrasion fatigue. [H] Upturned plates and adhering particles evidencing abrasion fatigue. Images were taken using a JEOL JSM-6480LV SEM. Terminology is after Vos et al. (2014).

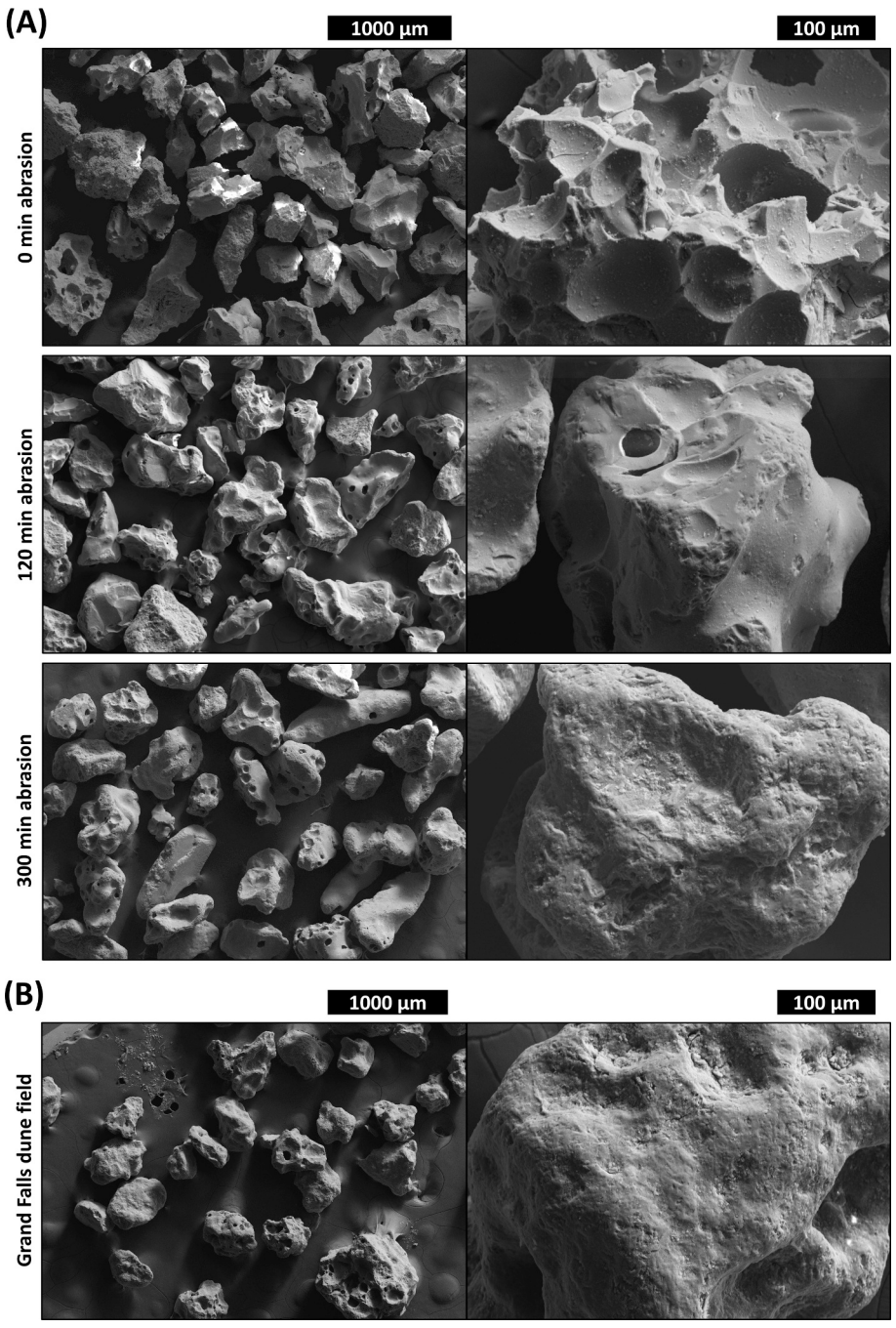

Fig. 6. SEM images of aeolian microtextures on basalt sand – SEM secondary electron images of microtextures on basaltic sand from SANDAR abrasion experiments and natural aeolian environments. [A] Basaltic tephra from Pisgah Crater in the Mojave Desert, California. Shown at two different scales before abrasion, after 120 min in the SANDAR, and after 300 min in the SANDAR. The initial grains are highly angular and sharp with smooth surfaces; after abrasion in the SANDAR, they become rounded and textured. [B] SEM secondary electron images of natural aeolian basaltic sand from Grand Falls dune field in Arizona. The natural sand shows similar microtextures to basalt that was abraded in the SANDAR, including rounded edges and low-relief texture. Images were taken using a Zeiss Supra40VP SEM.

improve capabilities for future sedimentary research on Earth and Mars. The SANDAR can be utilized in such research as an accessible, versatile device that simulates the aeolian transport of sediment. The SANDAR resolves several limitations of other experimental devices, resulting in improved and better-constrained experimental conditions. Benefits include (1) compatibility with large quantities of sediment (several grams) with grain sizes consistent with natural saltating sand; (2) well-constrained samples that allow for accurate measurements of dust production and grain size distribution over time; (3) the promotion of grain-to-grain collisions; and (4) the promotion of continuous sand circulation to support equal processing of all grains in a sample. A window into the abrasion chamber provides a view of experiments and enables the measurement of grain velocities.

The SANDAR is shown to achieve similitude of kinetic energy for natural saltating sand on both Earth and Mars. Indeed, it matches the kinetic energy of terrestrial and Martian saltation better than other experimental devices powered by air, paddle wheels, or gravity. Furthermore, the SANDAR is versatile and can be adapted to simulate a range of aeolian settings beyond those discussed here—including, potentially, other planetary bodies. Validation experiments demonstrate that both quartz and basaltic sand grains abraded in the SANDAR develop microtextures diagnostic of aeolian transport, indicating that

the SANDAR generates the same type of mechanical weathering as saltation. Thus, the SANDAR presents a valid option for future experimental research on aeolian abrasion and dust production.

CRediT authorship contribution statement

Anna E. Baker: Writing – review & editing, Writing – original draft, Visualization, Validation, Methodology, Investigation, Funding acquisition. **Devon M. Burr:** Writing – review & editing, Supervision, Resources, Project administration, Methodology, Investigation, Conceptualization. **Rachel L. Fry:** Writing – review & editing, Validation, Methodology, Investigation. **Joshua P. Emery:** Writing – review & editing, Supervision, Resources, Funding acquisition. **Mark J. Loeffler:** Writing – review & editing, Resources, Methodology.

Declaration of competing interest

The authors declare that they have no known competing financial interests or personal relationships that could have appeared to influence the work reported in this paper.

Acknowledgements

We gratefully acknowledge Vernon Rich and Gregory Florian for their aid with the design and construction of the mill body and metal components of the experimental device. Assistance with the SEM from Ronald Allen and Casey Tierney is also greatly appreciated. We thank Amber Gullikson and Timothy Titus of the U.S. Geological Survey Astrogeology Science Center for providing access to the Grand Falls dune field sediment, and we also thank the Leupp Chapter House for their support of scientific research at Grand Falls. Fieldwork on the Navajo Nation was conducted under a permit from the Navajo Nation Minerals Department. Any persons wishing to conduct geologic investigations on the Navajo Nation must apply for and receive a permit from the Navajo Nation Minerals Department, P.O. Box 1910, Window Rock, Arizona 86515, telephone # (928) 871-6587. Two anonymous reviews helped us improve this manuscript.

This work was funded by the National Science Foundation Graduate Research Fellowship Program (Award 1938054). Additional support was provided by the Arizona NASA Space Grant Consortium (Cooperative Agreement 80NSSC20M0041) and by the Geological Society of America Gould Research Grant. Any use of trade, firm, or product names is for descriptive purposes only and does not imply endorsement by the U.S. Government.

Appendix A. Supplementary data

Supplementary data to this article can be found online at https://doi.org/10.1016/j.aeolia.2025.101027.

Data availability

Data will be made available on request.

References

Adams, S.M., Soreghan, G.S., 2020. A test of the efficacy of sand saltation for silt production: Implications for the interpretation of loess. Geology 48 (11), 1105–1109.
Alfano, F., Ort, M.H., Pioli, L., Self, S., Hanson, S.L., Roggensack, K., Allison, C.M., Amos, R., Clarke, A.B., 2019. Subplinian monogenetic basaltic eruption of Sunset Crater, Arizona, USA. GSA Bulletin 131 (3–4), 661–674.
Anderson, G.E., 1926. Experiments on the rate of wear of sand grains. J. Geol. 34 (2), 144–158.
Anderson, R.S., 1986. Erosion profiles due to particles entrained by wind: Application of an eolian sediment-transport model. Geol Soc Amer Bull 97 (10), 1270–1278.
Andreotti, B., Claudin, P., Iversen, J.J., Merrison, J.P., Rasmussen, K.R., 2021. A lower-than-expected saltation threshold at Martian pressure and below. Proc Nat Acad Sci 118 (5), e2012386118.
Bagnold, R. A. (1941), The physics of blown sand and desert dunes: New York, William Morrow & Company.
Baker, A.E., Burr, D.M., Fry, R.L., McCanta, M.C., 2025. Experimental Investigation into the Maturation of Aeolian Sands on Mars. Paper Presented at 8th International Planetary Dunes Workshop.
Beladjine, D., Ammi, M., Oger, L., Valance, A., 2007. Collision process between an incident bead and a three-dimensional granular packing. Phys. Rev. E 75 (6), 061305.
Blatt, H., 1973. Origin of sedimentary rocks. Soil Sci. 115 (5), 400.
Bloore, F.J., 1977. The shape of pebbles. J. Int. Assoc. Math. Geol. 9, 113–122.
Bond, W.L., 1951. Making small spheres. Rev Sci Instruments 22 (5), 344–345.
Bourke, M.C., Edgett, K.S., Cantor, B.A., 2008. Recent aeolian dune change on Mars. Geomorphology 94 (1–2), 247–255.
Bourke, M.C., Lancaster, N., Fenton, L.K., Parteli, E.J., Zimbelman, J.R., Radebaugh, J., 2010. Extraterrestrial dunes: an introduction to the special issue on planetary dune systems. Geomorphology 121 (1–2), 1–14.
Brecker, J.N., 1974. The fracture strength of abrasive grains. J Eng Ind 96 (4), 1253–1257. https://doi.org/10.1115/1.3438503.
Bristow, C.S., Moller, T.H., 2018. Dust production by abrasion of eolian basalt sands: Analogue for Martian dust. J. Geophys. Res. Planets 123 (10), 2713–2731.
Bullard, J.E., McTainsh, G.H., Pudmenzky, C., 2004. Aeolian abrasion and modes of fine particle production from natural red dune sands: an experimental study. Sedimentology 51 (5), 1103–1125.
Bullard, J.E., McTainsh, G.H., Pudmenzky, C., 2007. Factors affecting the nature and rate of dust production from natural dune sands. Sedimentology 54 (1), 169–182.
Bullard, J.E., White, K., 2005. Dust production and the release of iron oxides resulting from the aeolian abrasion of natural dune sands. Earth Surface Proc Landforms 30 (1), 95–106.
Bullard, J.E., Zhou, Z., Davis, S., Fowler, S., 2022. Breakdown and modification of microplastic beads by aeolian abrasion. Env. Sci. & Tech. 57 (1), 76–84.
Burr, D.M., Finch, J.A., 2024. Seeking sand origins on Mars: Towards testing the volcaniclastic hypothesis globally. Icarus 420, 116194.
Burr, D.M., Nguyen, V.N.H., Gibson, T.M.G., Chinchkhede, T., 2024. Estimating grain sizes of Martian dune sand: a freeware-based methodology with initial results. Earth Space Sci. 11 (9), e2024EA003697.
Burr, D.M., Viviano, C.E., Michaels, T.I., Chojnacki, M., Jacobsen, R.E., 2022. An explosive volcanic origin identified for dark sand in Aeolis Dorsa, Mars. Geology 50 (8), 939–943. https://doi.org/10.1130/G49814.1.
Chamayou, A., Dodds, J.A., 2007. Air jet milling. Handbook of Powder Technology 12, 421–435.
Chojnacki, M., Burr, D.M., Moersch, J.E., Wray, J.J., 2014. Valles Marineris dune sediment provenance and pathways. Icarus 232, 187–219.
Cornwall, C., Bandfield, J.L., Titus, T.N., Schreiber, B., Montgomery, D., 2015. Physical abrasion of mafic minerals and basalt grains: Application to martian aeolian deposits. Icarus 256, 13–21.
Costa, P.J.M., Andrade, C., Dawson, A.G., Mahaney, W.C., Freitas, M.C., Paris, R., Taborda, R., 2012. Microtextural characteristics of quartz grains transported and deposited by tsunamis and storms. Sed. Geol. 275, 55–69.
Costa, P.J.M., Andrade, C., Mahaney, W.C., Da Silva, F.M., Freire, P., Freitas, M.C., Janardo, C., Oliveira, M.A., Silva, T., Lopes, V., 2013. Aeolian microtextures in silica spheres induced in a wind tunnel experiment: Comparison with aeolian quartz. Geomorphology 180, 120–129.
Costa, P.J.M., Park, Y.S., Kim, Y.D., Quintela, M., Mahaney, W.C., Dourado, F., Dawson, S., 2017. Imprints in silica grains induced during an open-channel flow experiment: Determination of microtextural signatures during aqueous transport. J Sed Res 87 (7), 677–687.
Creyssels, M., Dupont, P., El Moctar, A.O., Valance, A., Cantat, I., Jenkins, J.T., Pasini, J. M., Rasmussen, K.R., 2009. Saltating particles in a turbulent boundary layer: Experiment and theory. J. Fluid Mech. 625, 47–74.
Crouvi, O., Amit, R., Enzel, Y., Gillespie, A.R., 2010. Active sand seas and the formation of desert loess. Quat. Sci. Rev. 29 (17–18), 2087–2098.
Crouvi, O., Amit, R., Enzel, Y., Porat, N., Sandler, A., 2008. Sand dunes as a major proximal dust source for late Pleistocene loess in the Negev Desert, Israel. Quaternary Res. 70 (2), 275–282.
Crouvi, O., Schepanski, K., Amit, R., Gillespie, A.R., Enzel, Y., 2012. Multiple dust sources in the Sahara Desert: the importance of sand dunes. Geophys. Res. Lett. 39 (13).
Diniega, S., Burr, D.M., Chojnacki, M., Lapôtre, M.G.A., Swann, C., 2022. 7.23 -Martian Dunes: A Crucial Record of Present and past Mars Surface Environment and Aeolian Processes. In: Shroder, J.F. (Ed.), Treatise on Geomorphology (second Edition). Academic Press, Oxford, pp. 617–636. https://doi.org/10.1016/B978-0-12-818234-5.00177-2.
Domokos, G., Gibbons, G.W., Sipos, A.A., 2014. Circular, stationary profiles emerging in unidirectional abrasion. Math. Geosci. 46, 483–491.
Dutta, P.K., Zhou, Z., Dos Santos, P.R., Johnsson, M., Basu, A., 1993. A theoretical study of mineralogical maturation of eolian sand. Spec. Pap. Geol. Soc. Am. 203–203. https://doi.org/10.1130/SPE284-p203.
Edgar, J.O., Gould, J.A., Badreshany, K., Graham, S.P., Telling, J., 2024. Mineral abrasion experiments at Mars relevant temperatures. Icarus 422, 116238. https://doi.org/10.1016/j.icarus.2024.116238.
Ehlmann, B.L., Edgett, K.S., Sutter, B., Achilles, C.N., Litvak, M.L., Lapotre, M.G.A., Sullivan, R., Fraeman, A.A., Arvidson, R.E., Blake, D.F., 2017. Chemistry, mineralogy, and grain properties at Namib and High dunes, Bagnold Dune Field, Gale Crater, Mars: A Synthesis of Curiosity Rover Observations. J Geophys Res: Planets 122 (12), 2510–2543.

Ershov, D., Phan, M.-S., Pylvänäinen, J.W., Rigaud, S.U., Le Blanc, L., Charles-Orszag, A., Conway, J.R., Laine, R.F., Roy, N.H., Bonazzi, D., 2022. TrackMate 7: integrating state-of-the-art segmentation algorithms into tracking pipelines. Nat. Methods 19 (7), 829–832.
Fenton, L.K., Gullikson, A.L., Hayward, R.K., Charles, H., Titus, T.N., 2019. The Mars Global Digital Dune Database (MGD3): Global patterns of mineral composition and bedform stability. Icarus 330, 189–203.
Fenton, L.K., Hayward, R.K., Horgan, B.H., Rubin, D.M., Titus, T.N., Bishop, M.A., Burr, D.M., Chojnacki, M., Dinwiddie, C.L., Kerber, L., 2013. Summary of the Third International Planetary Dunes Workshop: Remote Sensing and image Analysis of Planetary Dunes, Flagstaff, Arizona, USA, June 12–15, 2012. Aeolian Res. 8, 29–38.
Forsman, N. F. (1978), Experimental eolian abrasion of very fine grains at different atmospheric pressures.
Forward, K.M., Lacks, D.J., Sankaran, R.M., 2009. Charge segregation depends on particle size in triboelectrically charged granular materials. Phys. Rev. Lett. 102 (2), 028001.
Greeley, R., Iversen, J.D., 1985. Wind as a Geological Process on Earth, Mars, Venus and Titan. Cambridge University Press, Cambridge. https://doi.org/10.1017/CBO9780511573071.
Greeley, R., Leach, R.N., Williams, S.H., White, B.R., Pollack, J.B., Krinsley, D.H., Marshall, J.R., 1982. Rate of wind abrasion on Mars. J. Geophys. Res. Solid Earth 87 (B12), 10009–10024.
Greeley, R., Kraft, M., 2001. Survivability of aggregate sands on Mars. Paper presented at Lunar Planet. Sci. Conf. 32nd,. Abstract #1839.
Grotzinger, J., Beaty, D., Dromart, G., Gupta, S., Harris, M., Hurowitz, J., Kocurek, G., McLennan, S., Milliken, R., Ori, G.G., 2011. Mars sedimentary geology: Key concepts and outstanding questions. Astrobiology 11 (1), 77–87. https://doi.org/10.1089/ast.2010.0571.
Guinness, E.A., Arvidson, R.E., Clark, I.H., Shepard, M.K., 1997. Optical scattering properties of terrestrial varnished basalts compared with rocks and soils at the Viking Lander sites. J. Geophys. Res. Planets 102 (E12), 28687–28703.
Gullikson, A.L., Titus, T.N., Hunter, M.A., 2023. In: PAAD: the Planetary Aeolian Analog Database. Terrestrial Analogs Data Portal, Flagstaff. https://doi.org/10.5066/P9IFVZEX.
Hayward, R.K., Mullins, K.F., Fenton, L.K., Hare, T.M., Titus, T.N., Bourke, M.C., Colaprete, A., Christensen, P.R., 2007. Mars global digital dune database and initial science results. J. Geophys. Res. Planets 112 (E11).
Hayward, R.K., Zimbelman, J.R., Fenton, L.K., Titus, T.N., Cushing, G.E., 2010. Mars Analog: Grand Falls Dune Field, Arizona, paper presented at Second International Planetary Dunes Workshop: Planetary Analogs-Integrating Models, Remote Sensing. and Field Data.
Henein, H., Brimacombe, J.K., Watkinson, A.P., 1983. Experimental study of transverse bed motion in rotary kilns. Metall. Trans. B 14, 191–205.
Ho, T.D., Valance, A., Dupont, P., Ould El Moctar, A., 2011. Scaling laws in aeolian sand transport. Phys. Rev. Lett. 106 (9), 094501.
Hooper, D.M., McGinnis, R.N., Necsoiu, M., 2012. Volcaniclastic aeolian deposits at Sunset Crater, Arizona: Terrestrial analogs for Martian dune forms. Earth Surf. Proc. Land. 37 (10), 1090–1105.
Kang, L., Guo, L., Gu, Z., Liu, D., 2008. Wind tunnel experimental investigation of sand velocity in aeolian sand transport. Geomorphology 97 (3), 438–450. https://doi.org/10.1016/j.geomorph.2007.08.018.
Knight, S.H., 1924. Eolian abrasion of quartz grains. Bull. Geol. Soc. Am. 35 (107), 8.
Kok, J.F., 2010. An improved parameterization of wind-blown sand flux on Mars that includes the effect of hysteresis. Geophys. Res. Lett. 37 (12).
Kok, J.F., Parteli, E.J., Michaels, T.I., Karam, D.B., 2012. The physics of wind-blown sand and dust. Rep. Prog. Phys. 75 (10), 106901.
Kok, J.F., Renno, N.O., 2009. A comprehensive numerical model of steady state saltation (COMSALT). J Geophys Res: Atmospheres 114 (D17).
Krinsley, D.H., Donahue, J., 1968. Environmental interpretation of sand grain surface textures by electron microscopy. Geol Soc Amer Bull 79 (6), 743–748.
Krinsley, D.H., Doornkamp, J.C., 1973. Atlas of quartz sand surface textures. Cambridge University Press.
Krinsley, D.H., Greeley, R., 1986. Individual particles and Martian aeolian action—A review. Sed. Geol. 47 (3–4), 167–189.
Krinsley, D.H., Greeley, R., Pollack, J.B., 1979. Abrasion of windblown particles on Mars—Erosion of quartz and basaltic sand under simulated Martian conditions. Icarus 39 (3), 364–384.
Krinsley, D.H., Leach, R., 1979. Simulated Martian aeolian abrasion of glassy basalt and augite, Rep Planet Geol. Program 311–312.
Krinsley, D.H., Takahashi, T., 1962. Surface textures of sand grains: an application of electron microscopy. Science 135 (3507), 923–925.
Kuenen, P. H. (1960b), Sand, Sci Amer, 202(4), 94-113.
Kuenen, P.H., 1960a. Experimental abrasion 4: Eolian action. J. Geol. 68 (4), 427–449.
Kuenen, P.H., 1962. Experimental abrasion 5: Frosting and Defrosting of Quartz Grains. J. Geol. 70 (6), 648–658.
Langevin, Y., Poulet, F., Bibring, J.-P., Gondet, B., 2005. Sulfates in the north polar region of Mars detected by OMEGA/Mars Express. Science 307 (5715), 1584–1586.
Lapotre, M.G.A., Ehlmann, B.L., Minson, S.E., Arvidson, R.E., Ayoub, F., Fraeman, A.A., Ewing, R.C., Bridges, N.T., 2017. Compositional variations in sands of the Bagnold Dunes, Gale Crater, Mars, from Visible-Shortwave Infrared Spectroscopy and Comparison with Ground Truth from the Curiosity Rover. J. Geophys. Res. Planets 122 (12), 2489–2509.
Mackie, D.S., Peat, J.M., McTainsh, G.H., Boyd, P.W., Hunter, K.A., 2006. Soil abrasion and eolian dust production: Implications for iron partitioning and solubility. Geochem., Geophys., Geosys. 7 (12).
Mahaney, W.C., 2002. Atlas of sand grain surface textures and applications. Oxford University Press.
Mangold, N., Baratoux, D., Arnalds, O., Bardintzeff, J.-M., Platevoet, B., Grégoire, M., Pinet, P., 2011. Segregation of olivine grains in volcanic sands in Iceland and implications for Mars. Earth Planet. Sci. Lett. 310 (3–4), 233–243.
Margolis, S.V., 1974. Processes of formation and environmental occurrence of microfeatures on detrital quartz grains. Amer. J. Sci. 274, 449–464.
Marshall, J., Fenton, L.K., Harlow, J.J.B., 2021. Limitations of applying grain weight similitude in aeolian studies with NASA Mars Wind Tunnel. Aeolian Res. 53, 100732. https://doi.org/10.1016/j.aeolia.2021.100732.
Marshall, J.R., Bull, P.A., Morgan, R.M., 2012. Energy regimes for aeolian sand grain surface textures. Sed. Geol. 253, 17–24.
Marvin, M.C., Hasson, M., Colicci, V., Abubo, R., Lapôtre, M.G., 2025. Microtextural analyses of detrital zircon for paleoenvironmental interpretations of metasedimentary rocks. Geology. https://doi.org/10.1130/G53712.1.
Massé, M., Bourgeois, O., Le Mouélic, S., Verpoorter, C., Spiga, A., Le Deit, L., 2012. Wide distribution and glacial origin of polar gypsum on Mars, Earth Planet Sci. Lett 317, 44–55.
Merrison, J., 2012. Sand transport, erosion and granular electrification. Aeolian Res. 4, 1–16.
Merrison, J.P., Gunnlaugsson, H.P., Jensen, S.K., Nørnberg, P., 2010. Mineral alteration induced by sand transport: a source for the reddish color of martian dust. Icarus 205 (2), 716–718.
Middleton, N.J., 2017. Desert dust hazards: a global review. Aeolian Res. 24, 53–63.
Miller, K.L., Szabó, T., Jerolmack, D.J., Domokos, G., 2014. Quantifying the significance of abrasion and selective transport for downstream fluvial grain size evolution. J. Geophys. Res. Earth 119 (11), 2412–2429.
Muhs, D.R., 2004. Mineralogical maturity in dunefields of North America, Africa and Australia. Geomorphology 59 (1–4), 247–269.
Nesbitt, H.W., Young, G.M., 1996. Petrogenesis of sediments in the absence of chemical weathering: Effects of abrasion and sorting on bulk composition and mineralogy. Sedimentology 43 (2), 341–358.
Nieter, W.M., Krinsley, D.H., 1976. The production and recognition of aeolian features on sand grains by silt abrasion. Sedimentology 23 (5), 713–720. https://doi.org/10.1111/j.1365 3091.1976.tb00104.x.
Nickling, W.G., Neuman, C.M., 2009. In: Aeolian Sediment Transport, in Geomorphology of Desert Environments. Springer, pp. 517–555.
Nitkiewicz, A., Sterner, S.M., 1988. An improved Bond air mill for the preparation of spherical single crystals. Amer. Mineral. 73 (5–6), 662–666.
O'Brien, P., McKenna Neuman, C., 2016. PTV measurement of the spanwise component of aeolian transport in steady state. Aeolian Res. 20, 126–138. https://doi.org/10.1016/j.aeolia.2015.11.005.
O'Hara-Dhand, K., Taylor, R., Smalley, I., Krinsley, D., Vita-Finzi, C., 2010. Loess and dust on Earth and Mars: Particle generation by impact mechanisms. Central European J of Geosci 2 (1), 45–51. https://doi.org/10.2478/v10085-010-0001-z.
Olivarius, M., Vosgerau, H., Nielsen, L.H., Weibel, R., Malkki, S.N., Heredia, B.D., Thomsen, T.B., 2022. Maturity matters in Provenance Analysis: Mineralogical differences Explained by Sediment Transport from Fennoscandian and Variscan sources. Geosciences 12 (8), 308.
Pettijohn, F.J., Potter, P.E., Siever, R., 1972. Sand and sandstone. Springer Science & Business Media.
Rasmussen, K.R., Sørensen, M., 2008. Vertical variation of particle speed and flux density in aeolian saltation: Measurement and modeling. J. Geophys. Res. Earth 113 (F2).
Rasmussen, K.R., Valance, A., Merrison, J., 2015. Laboratory studies of aeolian sediment transport processes on planetary surfaces. Geomorphology 244, 74–94.
Rogers, D., Christensen, P.R., 2003. Age relationship of basaltic and andesitic surface compositions on Mars: Analysis of high-resolution TES observations of the northern hemisphere. J. Geophys. Res. 108 (E4), doi:10.1029/2002JE001913.
Rumpel, D.A., 1985. Successive aeolian saltation: Studies of idealized collisions. Sedimentology 32 (2), 267–280.
Schindelin, J., Arganda-Carreras, I., Frise, E., Kaynig, V., Longair, M., Pietzsch, T., Preibisch, S., Rueden, C., Saalfeld, S., Schmid, B., 2012. Fiji: an open-source platform for biological-image analysis. Nat. Methods 9 (7), 676–682.
Shipley, S., Sarna-Wojcicki, A.M., 1983. Maps showing distribution, thickness, and mass of late Pleistocene and Holocene tephra from major volcanoes in the Pacific Northwest of the United States: A preliminary assessment of hazards from volcanic ejecta to nuclear reactors in the Pacific Northwest, Miscellaneous Field Studies Map 1435. US Geological Survey.
Smith, B.J., Wright, J.S., Whalley, W.B., 1991. Simulated aeolian abrasion of Pannonian sands and its implications for the origins of Hungarian loess. Earth Surf. Proc. Land. 16 (8), 745–752.
Stanev, R., Mitov, I., Specht, E., Herz, F., 2014. Geometrical Characteristics of the Solid Bed in a Rotary Kiln. Journal of Chemical Technology & Metallurgy 49 (1).
Stockstill-Cahill, K.R., Anderson, F.S., Hamilton, V.E., 2008. A study of low-albedo deposits within Amazonis Planitia craters: evidence for locally derived ultramafic to mafic materials. J. Geophys. Res. Planets 113 (E7).
Sullivan, R., Kok, J.F., 2017. Aeolian saltation on Mars at low wind speeds. J. Geophys. Res. Planets 122 (10), 2111–2143. https://doi.org/10.1002/2017JE005275.
Swann, C., Sherman, D.J., Ewing, R.C., 2020. Experimentally derived thresholds for windblown sand on Mars. Geophys. Res. Lett. 47 (3), e2019GL084484.
Sweeney, M.R., Lacey, T., Forman, S.L., 2023. The role of abrasion and resident fines in dust production from aeolian sands as measured by the Portable in situ Wind erosion Laboratory (PI-SWERL). Aeolian Res. 63, 100889.
Swet, N., Elperin, T., Kok, J.F., Martin, R.L., Yizhaq, H., Katra, I., 2019. Can active sands generate dust particles by wind-induced processes?, Earth Planet Sci. Lett 506, 371–380.

Swet, N., Kok, J.F., Huang, Y., Yizhaq, H., Katra, I., 2020. Low dust generation potential from active sand grains by wind abrasion. J. Geophys. Res. Earth 125 (7), e2020JF005545.
Szynkiewicz, A., Modelska, M., Buczyński, S., Borrok, D.M., Merrison, J.P., 2013. The polar sulfur cycle in the Werenskioldbreen, Spitsbergen: possible implications for understanding the deposition of sulfate minerals in the North Polar Region of Mars. Geochim. Cosmochim. Acta 106, 326–343.
Tirsch, D., Jaumann, R., Pacifici, A., Poulet, F., 2011. Dark aeolian sediments in Martian craters: Composition and sources. J. Geophys. Res. Planets 116 (E3).
Vos, K., Vandenberghe, N., Elsen, J., 2014. Surface textural analysis of quartz grains by scanning electron microscopy (SEM): from sample preparation to environmental interpretation. Earth Sci. Rev. 128, 93–104.
Weitz, C.M., O'Connell-Cooper, C., Thompson, L., Sullivan, R., Baker, M., Grant, J.A., 2022. The physical properties and geochemistry of grains on aeolian bedforms at Gale crater, Mars. J. Geophys. Res. Planets 127 (11), e2021JE007061.
Whalley, W.B., Smith, B.J., McAlister, J.J., Edwards, A.J., 1987. Aeolian abrasion of quartz particles and the production of silt-size fragments: Preliminary results. Geol Soc, London, Spec Pub 35 (1), 129–138.
White, B.R., Schulz, J.C., 1977. Magnus effect in saltation. J. Fluid Mech. 81 (3), 497–512.
White, B., Benzit, M., Bridges, N., 2006. Wind-tunnel Measurements of the Coefficient of Restitution and Kinetic Energy of Quartz Sand for Mars and Earth Impacting on a Basalt Rock with Numerical simulation. Paper Presented at 44th AIAA Aerospace Sciences Meeting and Exhibit.
Wright, J., Smith, B., Whalley, B., 1998. Mechanisms of loess-sized quartz silt production and their relative effectiveness: Laboratory simulations. Geomorphology 23 (1), 15–34.
Zhang, W., Wang, Y., Lee, S.-J., 2007. Two-phase measurements of wind and saltating sand in an atmospheric boundary layer. Geomorphology 88 (1), 109–119. https://doi.org/10.1016/j.geomorph.2006.10.017.
Zheng, X.-J., Fu, L.-T., Bo, T.-L., 2013. Incident velocity and incident angle of saltating sand grains on Mars. New J. Phys. 15 (4), 043014.
Zou, X.-Y., Wang, Z.-L., Hao, Q.-Z., Zhang, C.-L., Liu, Y.-Z., Dong, G.-R., 2001. The distribution of velocity and energy of saltating sand grains in a wind tunnel. Geomorphology 36 (3–4), 155–165.